

1 **COVID-19 Induced Fingerprints of a New Normal Urban Air Quality in the United States**

2 S. Kondragunta^{*1}, Z. Wei², B. C. McDonald³, D. L. Goldberg⁴, D. Q. Tong⁵

3 ¹NOAA NESDIS Center for Satellite Applications and Research, 5825 University Research
4 Court, College Park, MD

5 ²IM Systems Group, 5825 University Research Court, College Park, MD

6 ³NOAA Chemical Systems Laboratory, Boulder, CO

7 ⁴Milken School of Public Health, George Washington University, Washington, DC

8 ⁵Department of Atmospheric, Oceanic, and Earth Sciences, George Mason University, Fairfax,
9 VA

10
11
12
13
14
15
16
17
18
19
20
21
22
23
24
25
26
27

* Corresponding author: Phone: 301-655-7311. Email: Shobha.Kondragunta@noaa.gov

28
29
30
31
32
33
34
35
36
37
38
39
40
41
42
43
44
45
46
47
48
49
50
51

Abstract

Most countries around the world including the United States took actions to control COVID-19 spread that lead to an abrupt shift in human activity. On-road NO_x emissions from light and heavy-duty vehicles decreased by 9% to 19% between February and March at the onset of the lockdown period in the middle of March in most of the US; between March and April, the on-road NO_x emissions dropped further by 8% to 31% when lockdown measures were the most stringent. These precipitous drops in NO_x emissions correlated well with tropospheric NO₂ column amount observed by the Sentinel 5 Precursor TROPospheric Monitoring Instrument (S5P TROPOMI). Furthermore, the changes in TROPOMI tropospheric NO₂ across the continental U.S. between 2020 and 2019 correlated well with changes in on-road NO_x emissions ($r = 0.68$) but correlated weakly with changes in emissions from the power plants ($r = 0.35$). At the height of lock-down related unemployment in the second quarter of 2020, the NO₂ values decreased at the rate of 0.8 $\mu\text{moles}/\text{m}^2$ per unit percentage increase in the unemployment rate. Despite the lifting of lockdown measures, parts of the US continued to have ~20% below normal on-road NO_x emissions. To achieve this new normal urban air quality in the US, continuing remote work policies that do not impede economic growth may become one of the many options

Key Words: COVID-19, nitrogen dioxide, aerosol optical depth, TROPOMI, NO_x emissions, air quality, power plants

52 **Plain Language Summary**

53 This study documents the different phases of COVID-19 lockdown in 2020 and how
54 traffic emissions changed accordingly across the US, particularly in five different cities, namely
55 Los Angeles, San Francisco, San Joaquin Valley, New York City, and Atlanta. Analysis of data
56 for these cities from measurements on the ground and satellites indicate that a down turn in the
57 economy and telework policies reduced the number of cars and trucks on the road in March and
58 April due to which air quality got better. The recovery of traffic emissions after the lockdowns
59 were lifted was slow and below normal emissions were observed into the end of 2020. While the
60 cities in the east reached near normal levels, the west coast showed below normal traffic
61 emissions. The air quality in 2020 provided a window into the future as to how improvements
62 can be achieved.

63

64

65

66

67

68

69

70

71

72

73

74 1. Introduction

75 As the 2019 novel Corona virus (COVID-19) spread from China to other parts of the world,
76 various countries imposed lockdown measures one by one. Reports of improved air quality from
77 ground and satellite observations of aerosol optical depth (AOD) and nitrogen dioxide (NO_2)
78 soon followed in the media as documented by Kondragunta et al. (2020). The precipitous drops
79 seen in the tropospheric vertical column NO_2 (trop NO_2 here onwards) measured by the Sentinel
80 5P Tropospheric Monitoring Instrument (TROPOMI) were substantial, especially during the
81 strict lockdown period for each country (Gkatzelis et al., 2020). Goldberg et al. (2020) reported
82 that in the United States (US), trop NO_2 decreased by 9.2% to 45% in 26 cities from March 15 to
83 April 30, 2020 compared to the same period in 2019; these reported reductions account for the
84 influence of the weather. Other researchers reported similar findings, mainly reductions of
85 trop NO_2 attributed to reductions in traffic emissions both in the US. and across the globe in
86 major urban areas of Europe, India, and China (Bauwens et al., 2020; Keller et al., 2020; Zheng
87 et al., 2020; Vaderu et al., 2020; Straka et al., 2021; Nager et al., 2020). For example in
88 Washington D.C., average distance traveled by people dropped by 60% between February and
89 April when restrictions were fully in place (Straka et al., 2021). This sudden drop in trop NO_2 in
90 major metropolitan areas where the transportation source sector for NO_x ($\text{NO} + \text{NO}_2$) is strong is
91 due to reduced traffic on top of an already observed general decreasing trend in NO_x emissions.
92 According to Lamsal et al. (2015), trop NO_2 observed by the Ozone Monitoring Instrument
93 showed a decreasing trend with an overall decrease of 28% between 2005 and 2013. These
94 reductions are consistent with NO_x emissions reductions from major power plants in the US due
95 to the Clean Air Interstate Rule and Cross State Air Pollution Rule. The NO_x emissions

96 continued to drop as more and more power plants switched to natural gas or began to rely on
97 clean coal (de Gouw et al., 2014)

98 Nitrogen dioxide is released during combustion of fossil fuels and is a precursor for both
99 ozone and particulate matter, primary components of photochemical smog. Whether it enhances
100 or decreases ozone production is dependent on a given region being NO_x saturated or volatile
101 organic compound (VOC) saturated, due to the inherent non-linearity of ozone photochemistry
102 (Kroll et al., 2020; Mazzuca et al., 2016). The two main sources of NO₂ in the US are the energy
103 sector and the transportation sector according to the 2014 Community Emissions Data System
104 (Hoesly et al., 2018). A study by Zheng et al. (2020) analyzed the reductions in trace gas and
105 aerosol concentrations in China during the lockdown and found that the most significant drop in
106 aerosols was for nitrate aerosol. For the period corresponding to the lockdown in China, January
107 23 to February 22, 2020, mean nitrate aerosol concentration was 14.1 µg/m³; for the same period
108 in 2019, the concentration was 23.8 µg/m³. This 41% reduction is corroborated by reductions in
109 NO₂ observed by TROPOMI (Bauwens et al., 2020).

110 Though NO₂ is considered important due to its ozone and aerosol producing potential, it has
111 harmful human health impacts when inhaled. Achakulwisut et al (2019) showed that 64% of four
112 million pediatric asthma cases each year are due to exposure to NO₂. It should be noted though
113 that NO₂ was used as a proxy for traffic-related pollution. The World Health Organization
114 (WHO) standard for NO₂ is an annual average of 21 parts per billion and for the US, it is 53 parts
115 per billion. The authors do note that that daily exposures to NO₂ can vary from annual averages
116 and traffic pollution is usually a mixture of precursor gases, primary particulates, and
117 photochemically formed ozone and aerosols. Nevertheless, when countries went into lockdown,
118 the most noticeable indication of a drop in traffic related pollution is tropNO₂ in urban areas

119 observed by TROPOMI, lending support to the assumption that NO₂ is a good proxy for traffic
120 related pollution. The COVID-19 lockdown measures disproportionately impacted traffic more
121 than industrial operations.

122 We analyzed TROPOMI tropNO₂ and Suomi National Polar-orbiting Partnership Visible
123 Infrared Imaging Radiometer Suite (Suomi NPP VIIRS) AOD data in conjunction with on-road
124 NO_x emissions data, NO_x emissions from power plants, and unemployment rates where
125 available. The goal of this study is to examine the trends in on-road and power plant emissions
126 for five different locations (four urban areas and one rural area) to answer the questions: (1) are
127 changes in NO_x emissions during the lockdown detectable in TROPOMI tropNO₂ data, (2) are
128 the economic indicators consistent with emissions changes, and (3) did the trends reverse with
129 the lifting of lockdown measures in the major metro areas. These questions are answered with
130 spatial and temporal analysis of ground-based observations and satellite data, relating indicators
131 of human activity during and prior to COVID-19 lockdown with air quality, and examining if a
132 new normal urban air quality can be achieved with novel policies.

133 2. Methods

134 2.1. Sentinel 5P TROPOMI NO₂

135

136 The TROPOMI NO₂ algorithm is based on the Differential Optical Absorption
137 Spectroscopy technique that involves fitting the spectra in the NO₂ absorption region between
138 405 nm and 465 nm using known laboratory-measured reference absorption spectra. The
139 Sentinel 5P flies in formation with SNPP. Though some Sentinel 5P trace gas algorithm
140 retrievals depend on the VIIRS cloud mask, the NO₂ algorithm relies on cloud retrievals using its
141 oxygen A-band absorption (van Geffen et al., 2019). The cloud fraction and effective pressure

142 are used in air mass factor calculation for partially cloudy pixels. There is an indication that the
143 cloud algorithm is likely conservatively masking out good NO₂ retrievals according to a
144 validation study conducted by Judd et al. (2020). Though Judd et al (2020) used data with
145 quality flag equals to unity, we used the quality flag value (0.75) recommended by the NO₂
146 algorithm theoretical basis document (van Geffen et al., 2019). Only data with quality flag >
147 0.75 were used as this quality flag setting ensures that cloudy retrievals or retrievals with
148 snow/ice covered pixels are screened out. The TROPOMI Level 2 product file consists of pixel
149 level (3.5 km x 5.6 km) NO₂ tropospheric column amount which we used in this study. The NO₂
150 algorithm retrieves total column NO₂ and separates the stratosphere from troposphere using
151 chemical transport model predicted stratospheric NO₂ analysis fields (van Geffen et al., 2019).
152 The expected accuracy of the tropospheric NO₂ column for polluted regions with high NO₂
153 values is ~25% and independent validation efforts using ground-based spectrometers such as
154 Pandora have confirmed that tropNO₂ is generally under-estimated, especially in polluted regions
155 and that significant sources of errors come from coarser resolution a priori profiles used in the
156 retrieval algorithm (Chan et al., 2020). Comparisons of TROPOMI tropNO₂ column with
157 Pandora ground station retrievals of tropospheric NO₂ in Helsinki showed that mean relative
158 difference is $-28.2\% \pm 4.8\%$ (Ialongo et al., 2020). Similar comparisons between Pandora
159 ground station retrievals and tropNO₂ in Canada for urban (Toronto) and rural (Egbert) stations
160 show that tropNO₂ has a -23% to -25% bias for polluted regions and a 7% to 11% high bias in
161 rural region (Zhao et al., 2020). Sources of error in tropNO₂ include altitude dependent air mass
162 factors, stratosphere-troposphere separation of NO₂, a priori NO₂ profile and shape, surface
163 albedo climatology, and calibration errors as a function of view angle (van Geffen et al., 2019;
164 Judd et al., 2020; Ialongo et al., 20; Zhao et al., 2020; Chan et al., 2020). Judd et al. (2020)

165 showed that the TROPOMI NO₂ validation carried out during the Long Island Sound
166 Tropospheric Ozone Study (LISTOS) experiment showed that the TROPOMI tropNO₂ column
167 retrievals have a bias of -33% and -19% versus Pandora and airborne spectrometer retrievals
168 respectively. The biases improve to -19% and -7% when the TROPOMI NO₂ algorithm is run
169 with a priori profiles from a regional air quality model indicating that retrievals are very sensitive
170 to a priori profile. One aspect that is not fully explored by Judd et al. (2020) is the influence of
171 aerosols on air mass factor calculations. Research on aerosol impact on air mass factors
172 indicates that the effect of aerosols on NO₂ retrieval can vary depending on aerosol type
173 (absorbing or scattering), amount, and vertical location (is aerosol mixed in with NO₂ in the
174 boundary layer or is the layer detached from NO₂ layer) in the atmospheric column (Tack et al.,
175 2019; Judd et al., 2019; Liu et al., 2020; Lin et al., 2014).

176 The Level 2 TROPOMI NO₂ data were downloaded from the European Space Agency
177 datahub (<https://s5phub.copernicus.eu/dhus/#/home>).

178 The data for January to February 2020 is considered Business as Usual (BAU), the data
179 for 15 March to 30 April 2020 is considered the lockdown period, and the data for 1 May to
180 November 2020 is considered as representing the post lockdown period.

181 The TROPOMI data are available only from mid-2018 to the present. We removed the
182 seasonality in tropNO₂ data in two simple ways: by simply taking the difference between 2019
183 and 2020 for the same month so the sun-satellite geometries and weather conditions are similar
184 barring any unusual inter-annual variabilities, and by doing double differencing as described in
185 section 3.1.

186 2.2. On-road NO_x Emissions

187

188 The on-road emissions are obtained using the Fuel-based Inventory of Vehicle Emissions
189 (FIVE) where vehicular activity is estimated using taxable fuel sales for gasoline and diesel fuel
190 reported at a state-level and downscaled to the urban scale using light- and heavy-duty vehicle
191 traffic count data (McDonald et al., 2014). Once the fuel use is mapped, NO_x emissions are
192 estimated using fuel-based emission factors (in g/kg fuel) based on roadside measurements or
193 tunnel studies (Hassler et al., 2016; McDonald et al., 2012; McDonald et al., 2018). The emission
194 factors are calculated separately for light-duty gasoline vehicles and heavy-duty diesel trucks.
195 The FIVE methodology was developed to derive traffic emissions to study their impact on air
196 quality (Kim et al., 2016; McDonald et al., 2018), but in the case of 2020, the fuel-based
197 methods provide evidence for quantifying the impact of reduced human activity during the
198 lockdown period on air pollutant emissions (e.g., NO_x).

199 Here, we downscale on-road gasoline and diesel fuel sales following McDonald et al. (2014)
200 for our 2019 base year, which is treated as the BAU case. We have chosen to focus on four US
201 urban areas where real-time traffic counting data are publicly available, including the South
202 Coast air basin (Los Angeles county, Orange county, and portions of Riverside and San
203 Bernardino counties), San Francisco Bay Area (Marin, Sonoma, Napa, Solano, Contra Costa,
204 Alameda, Santa Clara, San Mateo, and San Francisco counties), New York City (Richmond,
205 New York, Kings, Queens, and Bronx counties), and the Atlanta metropolitan region (Cherokee,
206 Clayton, Cobb, Coweta, Dekalb, Douglas, Forsyth, Fulton, Gwinnett, Henry, Rockdale, and
207 Spalding counties). We also include one rural region for contrast, the San Joaquin Valley in
208 California (Fresno, Kern, Kings, Madera, Merced, San Joaquin, Stanislaus, and Tulare counties).
209 For the BAU case, we account for typical seasonal and day-of-week activity patterns of light-
210 and heavy-duty vehicles separately). For the COVID-19 case, we scale the January BAU

211 emissions case with real-time light- and heavy-duty vehicle traffic counting data for the year
212 2020, which are described in Harkins et al. (2020). Light-duty vehicle counts are used to project
213 on-road gasoline emissions and heavy-duty truck counts for on-road diesel emissions during the
214 pandemic.

215 To estimate NO_x emissions, the FIVE NO_x emission factors have been updated to 2019 based
216 on the regression analyses of roadway studies (Hassler et al., 2016; McDonald et al., 2012;
217 McDonald et al., 2018), and we use a value of running exhaust emission factors of 1.7 ± 2 g
218 NO_x/kg fuel and 12.4 ± 1.9 g NO_x/kg fuel for on-road gasoline and diesel engines, respectively.
219 Cold-start emissions are scaled relative to the running exhaust emissions based on the US
220 Environmental Protection Agency (EPA) MOVES2014 model (EPA, 2015). We use the 2019
221 NO_x emission factor for both the BAU and COVID-19 adjusted cases. Thus, the differences in
222 the BAU and COVID-19 cases are only due to changes in traffic activity. We use the same
223 emission factor for 2019 and 2020 because past studies have shown during the 2008 Great
224 Recession the turnover of the vehicle fleet and corresponding reductions in emission factors are
225 slower (Bishop and Steadman, 2014). Total on-road NO_x emissions are the sum of emission
226 estimates for light-duty vehicles and heavy-duty trucks. The off-road mobile source emissions
227 are not included in the dataset. In cities, on-road transportation accounts for as much as 75% of
228 the NO_x emissions (Kim et al., 2016), and is a critical emissions sector to quantify.

229 Uncertainties in FIVE on-road emission estimates arise from non-taxable fuel sales associated
230 with off-road machinery, and from mismatches where fuel is sold and where driving occurs,
231 though diesel fuel sales reports are adjusted based on where long-haul trucking occurs
232 (McDonald et al., 2014). However, the main source of uncertainty is the accuracy of fuel-based
233 emissions factors used to calculate co-emitted air pollutant species (McDonald et al., 2018). The

234 underlying traffic counting data are available at hourly time resolution; however, here we have
235 averaged the data to daily averages. Jiang et al. (2018) report the uncertainty in fuel sales (3%-
236 5%) and NO_x emission factors (15%-17%) for on-road transportation.

237 2.3. Power Plant NO_x Emissions

238 The daily power plant NO_x emissions were obtained from the US EPA Continuous Emissions
239 Monitoring System (<https://www.epa.gov/airmarkets>) and the energy generation/consumption
240 statistics were obtained from the Energy Information Administration (eia.gov). Unlike the traffic
241 emissions, power plant emissions did not change much during the lockdown. Power generation
242 from fossil fuels dropped from 38,332 Gwh in March to 29,872 Gwh in April and rebounded to
243 pre-pandemic levels by June. The total NO_x emissions in the US from power plants dropped
244 from 54,531 tons in March to 44,016 tons in April, a 19% decrease. This may seem like a big
245 drop in production but the absolute values are quite small. For example, NO_x emissions from
246 power plants within the 75 km of Los Angeles emitted only 20 tons in March 2020. For January
247 to July, nationally, total NO_x emissions from power plants were 0.8 and 0.67 million metric tons
248 in 2019 and 2020 respectively. This is a 16% reduction compared to 50% reduction in on-road
249 emissions, for the same months between 2019 and 2020.

250 In contrast, on-road emissions from vehicles in the Los Angeles area alone emitted nearly
251 5,367 tons of NO_x. Power plant NO_x emissions in the US have decreased substantially over the
252 last two decades; they dropped by 86% between 1990 and 2019. This is due to the shift from
253 fossil fuels to other alternate energy sources for power generation. For example, the use of coal
254 as a source of electricity generation went down from 51% in 2001 to 23% in 2019 while the
255 natural gas as a source increased from 17% in 2001 to 38% in 2019. In our analysis, comparing
256 and contrasting NO_x emissions from on-road traffic and power plants for the six locations of

257 interest, we considered only the power plants within 75 km radius of the center of the city
258 location being analyzed.

259 2.4. Suomi National Polar-orbiting Partnership Visible Infrared Imaging Radiometer 260 Suite (SNPP VIIRS)

261
262 NOAA currently has two VIIRS instruments in orbit - one on SNPP launched on 28
263 October, 2011 and one on NOAA-20 launched on 18 November, 2017. The two VIIRS
264 instruments continuously observe the Earth with a 50-minute time difference and provide AOD
265 retrievals for cloud/snow-free scenes during the sunlit portion of the day. The VIIRS
266 instruments have 22 bands with 16 of the bands in the visible to long-wave infrared at moderate
267 resolution (750m), five bands at imager resolution (375m) covering 0.64 μ m, 0.865 μ m, 1.6 μ m,
268 3.74 μ m, and 11.45 μ m, and one broad Day-Night-Band (DNB) band centered at 0.7 μ m. The
269 NOAA AOD algorithm over ocean is based on the Moderate Imaging Spectroradiometer
270 (MODIS) heritage and for over land, the algorithm derives AOD for both dark targets as well as
271 bright surfaces (Levy et al., 2007; Laszlo and Liu, 2016; Zhang et al., 2016; Huang et al.,
272 2016). For this study, we used the SNPP VIIRS AOD because SNPP flies in formation with S5P
273 TROPOMI with a local equator crossing time of 1:30 PM and less than three minutes difference
274 in overpass time. The SNPP VIIRS AOD product has been extensively validated by comparing
275 it to Aerosol Robotic Network (AERONET) AODs and the VIIRS 550nm AOD is shown to have
276 a global bias of -0.046 ± 0.097 for AODs over land less than 0.1 and for AODs between 0.1 and
277 0.8, the bias is -0.194 ± 0.322 . In the US., for VIIRS AODs ranging between 0.1 and 0.8, the bias
278 is -0.008 ± 0.089 and for AODs greater than 0.8, the bias is about 0.068 ± 0.552 (Zhang and
279 Kondragunta, 2021). For the analysis of AOD data in this study, we remapped the high quality
280 (Quality Flag equals 0) 750m resolution AOD retrievals to $0.05^\circ \times 0.05^\circ$ resolution with a

281 criterion that for a grid to have a mean AOD value, there should be a minimum of 20% 750m
282 pixels with high quality AODs.

283 2.5. Unemployment Rate

284

285 The civilian labor force and unemployment estimates for metropolitan areas were obtained
286 through the Local Area Unemployment Statistics (LAUS) provided by the Bureau of Labor
287 Statistics (bls.gov). The LAUS program is a federal-state cooperative effort in which monthly
288 estimates of total employment and unemployment are prepared for over 7,500 areas including
289 metropolitan areas. The seasonal adjustments are carried out by the Current Employment
290 Statistics State and Area program (CES) using the statistical technique Signal Extraction in Auto
291 Regressive Integrated Moving Average Time Series (SEATS). These datasets are smoothed
292 using a Reproducing Kernel Hilbert Space (RKHS) filter after seasonal adjustment. The details
293 of the data collection, processing and release can be found at
294 <https://www.bls.gov/lau/laumthd.htm>. The data for January to November 2020 are used in this
295 study. To compare the NO₂ variation in metropolitan areas, the TROPOMI tropNO₂
296 column amounts were averaged inside each metropolitan area. The 1:500,000 polygon shape
297 files were used to test if a TROPOMI pixel is inside or outside a metropolitan area. The shape
298 files are from United States Census Bureau ([https://www.census.gov/geographies/mapping-](https://www.census.gov/geographies/mapping-files/time-series/geo/cartographic-boundary.html)
299 [files/time-series/geo/cartographic-boundary.html](https://www.census.gov/geographies/mapping-files/time-series/geo/cartographic-boundary.html)).

300 2.6. Matchup Criteria

301

302 The NO₂ data were matched to the on-road mobile emissions data for statistical and trend
303 analysis with certain criteria. Prior to generating the matchups, rotated wind analysis was carried
304 out on the original pixel level data. It is important to do this when sampling the satellite data

305 because NO_2 concentrations accumulate in the cities when wind speed is low and disperse away
306 from the city when wind speed is high. The satellite data are observed once a day in the mid-
307 afternoon whereas on-road mobile emissions represent daily values. To have representative
308 sampling, it is common to rotate the satellite pixel-level data in the direction of the wind
309 (Fioletov et al., 2015; Lorente et al., 2019; Goldberg et al., 2019; Zhao et al., 2020). We used the
310 European Center for Medium range Weather Forecast (ECMWF) Re-Analysis (ERA5) 30-km
311 resolution global wind fields (Hersbach et al., 2020). To do the wind rotation, each TROPOMI
312 pixel was collocated to ERA5 with tri-linear interpolation method in both temporal and
313 horizontal directions. The wind profiles were merged to the location of the TROPOMI pixel
314 center. The east-west (U) and north-south (V) wind speed components were averaged through
315 the vertical distribution within the bottom 100 hPa, approximated to be within the boundary
316 layer. Then, each TROPOMI pixel was rotated and aligned with the average wind direction from
317 the city center. The rotated pixels are gridded with 5 km x 5 km resolution to generate monthly
318 mean values for correlation analysis with on-road NO_x emissions.

319 Once the pixels are rotated, they are sampled for 100 km in the downwind direction, 50 km
320 in the upwind direction, and the cross-wind direction. This way, the elevated concentrations of
321 NO_2 moving away from the city in the downwind direction are captured. Figure 1a shows an
322 example of the TROPOMI NO_2 tropospheric column amount with Los Angeles as the focus.
323 The NO_2 data shown are monthly mean values for January 2020 remapped to a fixed grid. The
324 black rectangle shows the area of interest over Los Angeles that we want to compare with on-
325 road emissions. The ERA5 wind vectors are plotted on the NO_2 map to show wind direction. To
326 do the wind rotation, daily NO_2 pixel level data are first remapped to a 5 km x 5 km fixed grid
327 resolution. The grids are then rotated to align with the wind direction with downwind direction

328 pointing North (Figure 1b). The daily rotated grid values of NO₂ in 5 km x 5 km are averaged
329 over a month to generate a monthly mean. The monthly mean values can vary quite a bit
330 depending on missing data due to screening for the high quality data as well as cloud cover. In a
331 given month, the number of pixels with valid retrievals for a particular city can vary from 2% to
332 100% depending on cloud and snow cover; the mean values vary depending on the location of
333 the missing values, if they are in the center of the city where NO₂ is usually high or on the edges
334 of the city where NO₂ values can be low depending on wind speed and direction. In our analysis
335 for this study, prior to computing the monthly mean, the criterion we employed is that on a given
336 day, there should be a minimum of 25% of pixels in a region selected for matchups of satellite
337 data should have valid retrievals. The 25% threshold is a reasonable compromise because any
338 value higher than that will reduce the sample size (number of days included in the monthly
339 mean).

340 3. Results

341 3.1. Deseasonalizing tropNO₂ data

342

343 As already shown by many research studies, the global tropNO₂ column amounts dropped in
344 coincidence with partial or complete lockdowns during the height of the COVID-19 pandemic in
345 different parts of the world and in the US. In order to remove the seasonality from the signal,
346 researchers in these studies have adopted different approaches including the use of numerical
347 models to simulate the seasonality (e.g., Goldberg et al., 2020; Silver et al., 2020; Liu et al.,
348 2020). Seasonality should be accounted for because in the northern hemisphere winter months,
349 NO₂ amounts are higher than in summer months; as a result, during the transition from winter to
350 summer, NO₂ amounts are higher in February than in March. In our study, we used a double
351 differencing technique to account for seasonality. Consistent with Goldberg et al. (2020), we

352 used 1 January to 29 February 2020 as pre-lockdown period and 15 March to 30 April as the
353 lockdown period. The difference in mean tropNO₂ between lockdown and pre-lockdown is
354 referred to as 2020 Δ NO₂. For the same two corresponding periods in 2019, the difference in
355 mean tropNO₂ is referred to as 2019 Δ NO₂. Then, the difference of 2019 Δ NO₂ and 2020 Δ NO₂
356 was computed to tease out the changes in NO₂ due to reductions in emissions during the
357 lockdown (Δ tropNO₂). It should be noted though that the double differencing only removes the
358 seasonality and does not fully account for differences in meteorological events such as
359 precipitation or anomalously cold or hot conditions in one year versus the other but on a monthly
360 time scale they are minimized.

361 Figure 2a-b shows 2019 Δ NO₂ and 2020 Δ NO₂ which includes changes due to seasonality and
362 any changes due to emissions either from natural sources such as fires or from anthropogenic
363 urban/industrial sources. Figure 2c shows Δ tropNO₂ for the CONUS due to just changes in
364 emissions between the pre-lockdown and lockdown periods in 2020 with the seasonality
365 removed. Comparing Figure 2a and 2b, one can deduce that reductions in tropNO₂ between pre-
366 lockdown and lockdown are much stronger in 2020 compared to 2019. However, the double
367 difference plot in Figure 2c shows how much of that reduction seen in 2020 Δ NO₂ (Figure 2b) is
368 due to changes in emissions. The tropNO₂ changes are smaller in Figure 2c than in Figure 2b,
369 both in magnitude as well as spatial extent of the reductions.

370 The lockdown measures in most states in the US began in the middle of March 2020. The
371 first state to institute stay-at-home measures was California on 19 March and the last state was
372 Missouri on 6 April. The cities/regions with worse traffic related ozone pollution levels based on
373 the monitoring data from 2016-2018 compiled by the American Lung Association and the
374 duration for which they were in a lockdown are shown in Table 1. For regions that fall into

375 different states (e.g., Washington-Baltimore-Arlington), the dates for the state that had the
376 longest duration of lockdown are listed in the table. Most states were in a lockdown mode only
377 for one to two months and given the varying nature of the lockdown in different parts of the
378 country, we treated 15 March and 30 April as lockdown months. As shown in Figure 2a,
379 2019 Δ NO₂ is positive in some areas and negative in some areas whereas in 2020 (Figure 2b),
380 large negative values (reductions) are observed in most of the CONUS except in the Great Plains
381 region and the Pacific North West. These reduced tropNO₂ amounts are attributed to reduced
382 emissions due to lockdowns. Changes in the rural areas (either positive or negative) of the US
383 could be due to changes to natural sources such as soil and lightning NO_x emissions or due to
384 meteorological differences that the double differencing technique did not account for.

385 Fei Liu et al. (2021) used NASA global photochemical model simulations to study how long
386 the tropNO₂ data need to be averaged to minimize the influence of meteorological variability.
387 They simulated January 2019 to December 2020 by keeping the NO_x emissions the same
388 between the two years. and found that averaging the data over 31 days for the US leads to
389 differences in tropNO₂ between 2019 and 2020 less than 10%. Our double differencing was
390 done with tropNO₂ data averaged over 1.5 months which should substantially minimize the
391 differences in meteorology.

392 To confirm our results, we also repeated the analysis for a longer period and found that our
393 conclusions did not change. Setting the pre-lockdown period as 1 January to 15 March and the
394 lockdown period as 16 March to 30 May, and we found that tropNO₂ decreases are consistent
395 with those shown in Figure 2a-c (Figure S1a-c). We also applied scaling factors to account for
396 seasonality and meteorological variability developed by Goldberg et al. (GRL, 2020). These
397 scaling factors normalize tropNO₂ data to conditions of a typical week day based on TROPOMI

398 tropNO₂ data from 2018-2019, based on sun angle, wind speed, wind-direction, and day-of-
399 week. Figure S2 shows this analysis using the normalized tropNO₂ to investigate NO_x trends; it
400 shows reductions in tropNO₂ for different cities during the lockdown period that are consistent
401 with the double differencing analysis.

402 3.2. On-road NO_x emissions and tropNO₂

403

404 Focusing on the regions of interest with on-road NO_x emissions available for this study, we
405 calculated reductions in tropNO₂ for Los Angeles, Atlanta, San Francisco, San Joaquin Valley,
406 and New York City. As shown in Table 2, the largest reductions in tropNO₂ were observed for
407 New York City (-28%) and the smallest reductions were observed for San Joaquin Valley (-
408 17%). The largest reductions in NO_x emissions were also for New York City but the smallest
409 reductions were Atlanta followed by San Joaquin Valley. The 22% reductions in tropNO₂
410 observed for Los Angeles is due to nearly 50% reductions in on-road NO_x emissions. Without
411 accounting for the seasonality/meteorological differences between 2020 and 2019, the tropNO₂
412 reductions are 60%. This elucidates the need to account for differences in seasonality and
413 meteorology when analyzing the data for trends.

414 Goldberg et al (2020) reported tropNO₂ reductions of 20.2%, 18%, and 39% for Atlanta,
415 New York, and Los Angeles respectively and their analysis is also for a lockdown period
416 spanning 15 March to 30 April, 2020. Our analysis shows that tropNO₂ reductions for these
417 three cities are 21%, 17%, and 22%. Though the methodology used to remove the seasonality is
418 different, the reductions in tropNO₂ from our analysis and that of Goldberg et al. (2020) are
419 similar, with Los Angeles showing the biggest drop in tropNO₂ due to lockdown measures.

420

421 Figure 3 shows the time series of on-road mobile (cars and trucks combined) and power plant
422 NO_x emissions for the five different cities/regions in the US from January to November 2020;
423 the exception is New York City for which the time series ends on 31 August due to the non-
424 availability of traffic data. For Los Angeles, daily NO_x emissions are near 200 tons/day prior to
425 lockdown with values slightly lower on weekends (~150 tons/day). The Los Angeles basin is
426 home to 17 million people with 11.3 million cars; cars, trucks, and other off-road machinery
427 contributing to 80% of the observed NO_x in a typical year according to the 2019 emissions report
428 by South Coast Air Quality Management District ([http://www.aqmd.gov/docs/default-](http://www.aqmd.gov/docs/default-source/annual-reports/2019-annual-report.pdf?sfvrsn=9)
429 [source/annual-reports/2019-annual-report.pdf?sfvrsn=9](http://www.aqmd.gov/docs/default-source/annual-reports/2019-annual-report.pdf?sfvrsn=9)). Due to the lockdown and stay at home
430 orders, people stopped driving and NO_x emissions quickly began dropping on 19 March 2020;
431 the NO_x emissions begin to increase on 16 April 2020, even before the lockdown was lifted on 4
432 May. The lowest weekday NO_x emissions, 141.3 tons/day, occurred on 6 April. Even though
433 the NO_x emissions began to recover in the post lockdown period, they were still lower than the
434 pre-lockdown values. Compared to on-road emissions, power plant emissions are negligible for
435 the Los Angeles area. Power plants in the vicinity of Los Angeles (~75 km radius) emit only
436 ~0.8 tons per day on average compared to 200 tons per day emitted by on-road vehicles during
437 the pre-lockdown period on weekdays. On weekends, on-road emissions are lower (~150 to 175
438 tons/per day depending on whether it is a Saturday or Sunday) due to lower truck traffic (Marr
439 and Harley, 2002), whereas power plant emissions do not have any weekday/weekend
440 differences.

441 The NO_x emissions for the New York area encompass an area covering about 1,213 square
442 kilometers. The city is home to 8.34 million people but there are only 1.9 million vehicles (230
443 cars per 1000 people) because of the reliance on public transportation, a factor of three lower

444 than for Los Angeles, which has 660 cars per 1000 people. Similar to Los Angeles, the NO_x
445 emissions dropped in New York on 21 March when lockdown measures began. The pre-
446 lockdown levels of NO_x emissions are on average ~125 tons/day. It should be noted that New
447 York City is in the downwind region of NO_x emissions from New Jersey and Pennsylvania and
448 it is the recipient of regionally transported pollution (Tong et al., 2008). Unlike in the Los
449 Angeles metro area, the power plant emissions are higher but showed no trend similar to on-road
450 emissions. It is noteworthy that there was a jump in power plant emissions towards the end of
451 June which coincided with the opening of retail establishments on 22 June; the power plant
452 emissions in the New York City are higher in the summer than in winter, associated with
453 increased demand for air conditioning.

454 The NO_x emissions for the metro Atlanta area are similar to New York City but with a weak
455 weekday/weekend cycle. The Atlanta region encompassing Cherokee, Clayton, Cobb, Coweta,
456 Dekalb, Douglas, Forsyth, Fulton, Gwinett, Henry, Rockdale, and Spalding counties is about
457 3,695 square kilometers and is home to nearly five million people. The pre-lockdown levels of
458 NO_x emissions were on average ~125 tons/day. The metro Atlanta region is three times larger
459 than the area of New York City but the NO_x emissions are similar in magnitude. The state of
460 Georgia where Atlanta is located never went into a prolonged lockdown. Though the mayor of
461 Atlanta ordered people not to gather in large groups beginning 15 March and the Governor of
462 Georgia ordered bars and clubs to close on 24 March, schools were not closed until 1 April;
463 shelter in place was implemented on 8 April but was lifted immediately with no real lockdown
464 until 1 May-23 May. Consistent with these policies, the on-road NO_x emissions were lowest on
465 23 March (88.5 tons/day) and 26 May (74.5 tons/day) and returned to pre-lockdown levels at the
466 start of 1 June. The lowest on-road NO_x emission value, 74.5 tons, was observed on 26 May,

467 towards the end of the shelter in place orders. By 1 June, NO_x emissions values returned to pre-
468 lockdown levels in Atlanta.

469 For the pre-lockdown period, the weekday/weekend difference in NO_x emissions is larger in
470 New York City than in Los Angeles and Atlanta areas, due to commuter travel. The mean
471 difference in NO_x emissions between weekdays and Sundays (emissions are the lowest on
472 Sundays of each week) prior to the lockdown in the Los Angeles, New York, and Atlanta are
473 54.4 tons/day (26%), 65.4 tons/day (51%), and 41.1 tons/day (33%) respectively.

474 The San Joaquin valley is a 60,000 km² area that includes the population centers of
475 Bakersfield and Fresno as well as major freeway corridors, including I-5 and CA-99. Due to the
476 large geographic size of the San Joaquin Valley, the emissions magnitude is comparable to urban
477 centers. The San Joaquin Valley NO_x emissions remained consistent at ~55 tons/day throughout
478 the year with a very weak weekday/weekend cycle. Similar to Los Angeles, power plant
479 emissions are insignificant.

480 For the San Francisco Bay area, the on-road NO_x emissions are higher than the San Joaquin
481 Valley region but lower than in Los Angeles. The daily average NO_x emissions prior to the
482 lockdown were ~90 tons/day and there was a small drop in emissions (-33.2 tons/day) on 6 April
483 with a trend to return to normal by mid-April. The post lockdown NO_x emissions were lower
484 than pre-lockdown values for San Francisco as well.

485 3.3. Correlation between on-road NO_x emissions and tropNO₂

486

487 Given the knowledge of changes in on-road emissions in the five cities due to lockdown, we
488 wanted to examine if tropNO₂ shows similar behavior by exhibiting a linear relationship, and if
489 so demonstrate that the period for which the lowest NO_x emissions were observed in traffic data

490 also corresponds to the lowest observed tropNO₂ data. Additionally, we wanted to check if the
491 post lockdown recovery in traffic emissions is reflected in tropNO₂ data. We first examined the
492 direct relationship between daily tropNO₂ and daily on-road NO_x emissions for the five
493 locations; but only the analysis for Los Angeles is shown in Figure 4 for illustration purpose;
494 data from other cities showed similar behavior. The tropNO₂ and NO_x emissions for January and
495 February 2020, representing the BAU, and for March through November 2020 are shown in
496 Figure 4a and Figure 4b respectively. The coincident observations of tropNO₂ amount sampled
497 in the predominant wind direction are linearly correlated with on-road NO_x emissions but the
498 correlation is weak ($r=0.39$). The traffic emissions fall into three clusters corresponding to
499 emissions on Sundays (~150 tons/day), Saturdays (~180 tons/day), and weekdays (~199
500 tons/day) with minimal variability in each cluster whereas tropNO₂ amount varies between 50
501 and 225 $\mu\text{moles}/\text{m}^2$.

502 The variability in tropNO₂ can be attributed due to different reasons. First, the day to day
503 variability in cloud cover can lead to gaps in data. We used the recommended quality flag
504 threshold of 0.75 to screen out the data that has potential contamination from clouds but this
505 strict screening reduces the number of retrievals for a given location. Second, there is also
506 variability in the background NO₂ contribution to the tropospheric NO₂ column due to which
507 column NO₂ does not correlate well with NO_x emissions from sources on the ground. We
508 analyzed the background NO₂ signal in the tropospheric column amount for TROPOMI for 2019
509 and 2020 using Silvern et al. (2019) method and found it to be higher due to the longer winter-
510 time lifetime (lower temperature, weak photolysis, stronger wind dispersion, and less wet
511 scavenging) and lower in the summer with monthly mean values ranging between 15 and 20
512 $\mu\text{moles}/\text{m}^2$ (Figure S3). Sources of background NO₂ are soil emissions of NO_x which are

513 amplified after precipitation events, lightning produced NO_x , and chemical decomposition of
514 peroxyacetyl and alkyl nitrates. Transport of NO_2 from rural areas can also enhance trop NO_2
515 values that may not correlate well with NO_x emissions from sources on the ground. Third, wind
516 speed and direction influence the mean tropospheric NO_2 computed for the Los Angeles basin
517 because if the wind speed is high, NO_2 is dispersed and transported away from the city and if
518 wind speed is low, NO_2 is accumulates in the city. Any variability associated with background
519 NO_2 is detected by TROPOMI and accounted for in the column NO_2 amount, but this has no
520 relation to the NO_x emissions from on-road sources on the ground. We did account for the
521 effects of wind in our matchups by sampling the data in the downwind direction but higher wind
522 speeds dilute the NO_2 concentrations observed by TROPOMI (Figure S4). Outlier values of
523 trop NO_2 values are between 20 and 30 $\mu\text{moles}/\text{m}^2$ even when on-road emissions are high
524 indicating TROPOMI retrievals that are either sampled after pollutants are washed out of the
525 atmosphere due to rain or on days when wind speeds are unusually high. Retrievals can also be
526 noisy and have errors associated with air mass factors and a priori profiles. Parker et al. (2020)
527 report that the Los Angeles basin was unusually wet in 2020, especially during the late March
528 and early April 2020. Other researchers who correlated daily surface observations of NO_2 and
529 TROPOMI trop NO_2 for 35 different stations in Europe reported similar findings and they found
530 that correlation improved after averaging the data to monthly time scales (Ialongo et al., 2020;
531 Cersosimo et al., 2020; Goldberg et al., 2020).

532 The comparison for the lockdown and post lockdown period of March through November is
533 shown in Figure 4b; the correlation remains the same ($r = 0.39$) but the one interesting feature is
534 that the trop NO_2 and on-road emissions are very small during the lockdown compared to the pre-
535 lockdown. Daily NO_x emissions on many days are between 100 and 150 tons after 14 March;

536 prior to that, the region was not under stay-at-home orders. The tropNO₂ never goes above 200
537 $\mu\text{moles}/\text{m}^2$ for this period. Compared to the pre-lockdown period, the on-road NO_x emissions
538 and tropNO₂ values shifted to lower values within each cluster (shown in blue for weekdays,
539 green for Saturdays, and red for Sundays). During the lockdown, one would anticipate that there
540 would not be any difference between weekday and weekend emissions but the difference is stark
541 and is reflected in tropNO₂ data as well.

542 In order to correlate the changes in on-road NO_x emissions with changes in tropNO₂ between
543 2019 and 2020 for each of the five regions in this study, we averaged daily NO_x emissions
544 values and tropNO₂ values for each month (January to November) and created an average value
545 of all the five regions combined for each month. Figure 5a shows the monthly mean trend plot
546 ΔNO_x and ΔtropNO_2 for January to November; on-road emissions and tropNO₂ dropped steadily
547 and hit the lowest values in March and April, consistent with the lockdown measures. The
548 recovery began in May and continued to November for on-road emissions but did not completely
549 recover to the pre-lockdown levels. However, the ΔtropNO_2 trend plot shows recovery up to
550 August and then begins to show a decline from September to November. This decline in
551 tropNO₂ is attributed to Los Angeles and San Francisco. Figure 5b shows the correlation of on-
552 road NO_x emissions changes (ΔNO_x) between 2020 and 2019 with the difference in tropNO₂
553 amounts between 2020 and 2019 (ΔtropNO_2). The NO_x emissions were lower in 2020 compared
554 to 2019 for all the months and all the cities. The positive linear correlation ($r = 0.68$) suggests
555 that TROPOMI tropNO₂ observations captured the changes in on-road emissions and can be
556 used to study the changes in NO_x emissions due to traffic elsewhere in the US where there are no
557 observations from the ground.

558 Even though traffic emissions are the dominant source for NO_x, there are power plants in the
559 vicinity of the cities emitting NO_x continuously and unlike traffic emissions they do not exhibit a
560 weekday/weekend cycle. Figure 6 shows a map of tropNO₂ for the second quarter in 2020
561 (April/May/June) with on-road emissions and power plant emission for each of the five analysis
562 cities as stacks. The locations of power plants in other parts of the country are circled in pink,
563 indicating that these power plants emit greater than 1500 tons in a given quarter; power plants
564 with lower monthly NO_x emissions (< 1500) tons are not shown on the map. It is difficult to
565 isolate the NO₂ plumes from power plants in urban areas in the TROPOMI tropNO₂ map as the
566 NO_x emitted from the power plants mixes and becomes indistinguishable from on-road
567 emissions. Consistent with this analysis, changes in NO_x emissions between 2020 and 2019 for
568 power plants within 75 km of each of the five analysis cities correlated weakly with changes in
569 tropNO₂ (Pearson correlation coefficient = 0.35); power plant NO_x emissions can explain only
570 12% of the variability seen in tropNO₂ (Figure 7). Also as can be seen in Figure 7, the daily
571 average changes in power plant emissions between 2020 and 2019 were positive for some plants
572 and negative for some but mostly varied between ±20 tons/day.

573

574 3.4. Correlation between tropNO₂ and AOD

575

576 The premise for the impact of NO_x emissions reductions on improved air quality due to
577 reduced human activity during the lockdown period depends on how the photochemical
578 processes changed compared to the BAU scenario. The photochemical production of ozone and
579 surface PM_{2.5} (particulate mass of particles smaller than 2.5 μm in median diameter) depends not
580 only on NO_x emissions but also on VOCs and their ratio (Baider et al., 2015; Parker et al., 2020;
581 McDonald et al., 2018; Qin et al., 2021). Most analysis of the impact of COVID-19 lockdowns

582 on air quality using satellite data have focused on TROPOMI NO₂ and attributed the reductions
583 of NO_x emissions to improved air quality; the reductions in VOC emissions are largely unknown,
584 especially from non-vehicular sources. Atmospheric formation of nitrate and organic aerosols is
585 driven by NO_x, VOCs, and ammonia emissions and if the photochemical processes are in a NO_x
586 limited or VOC limited regime. To analyze the AOD data for indications of reduced aerosol
587 formation due to reduced NO_x emissions, one complicated factor is the transport of smoke
588 aerosols from upwind regions and how the transported signal can be removed from the AOD
589 data. To address this issue, we tested the hypothesis that the AOD/NO₂ ratio is small when
590 pollution sources are local and high when non-local sources bring transported aerosols into the
591 domain. We calculated the weekly correlation between AOD and NO₂ and obtained the slope for
592 each week over one year in 2019 and 2020, to document the changes in slope as a function of
593 time during the year (Figure 8a-c); In Figure 8a-b, we show an example of how slopes are
594 derived using the scatter plot between VIIRS AOD and TROPOMI tropNO₂ for one week in
595 September 2019 and in 2020. For 2019, when the fire season was not a major contributing factor
596 to aerosol concentrations, the slopes are small in the winter months and slowly increase towards
597 the summer (Figure 8c). This is consistent with the knowledge that ammonium nitrate formation
598 peaks in the summer due to the availability of ammonia from increased agricultural activity and
599 higher volatility associated with higher temperatures (Schiferl et al., 2014).

600 The weekly scatter plots of AOD and tropNO₂ for September 2019 and 2020 in Figure 8a-b show
601 that the tropNO₂ values in both years ranged between 30 and 120 μmoles/m² whereas AOD
602 values in 2020 were much higher (between 0.2 and 0.9) compared to values in 2019 (between 0.1
603 and 0.2). The AOD values in the US typically range between 0 and 1, with higher AODs
604 typically observed in the presence of biomass burning smoke or dust storms. Given this

605 knowledge that slopes are higher when transported aerosol is involved, we were able to filter the
606 AOD data. The filtered data will be used in a future study to analyze trends in AOD due to NO_x
607 emissions reductions.

608 3.5. Correlation of tropNO₂ and Unemployment Rate

609
610 Because of the lockdown measures and work from home policies for majority of the
611 workplaces in the US, the service industry has suffered and the unemployment rate has risen.
612 The US unemployment rate increased from about 4.4% in March to 14.7% in April during the
613 first phase of lockdowns. The unemployment rate nationwide improved as the progressed but
614 certain parts of the country continued to experience a very high unemployment rate throughout
615 2020 (Figure 9). Amongst the employed, 28% of employees continued to work from home as of
616 November indicating that below normal NO_x emissions data are to be expected. The correlation
617 between unemployment rate and tropNO₂ for metropolitan areas with a pre-pandemic civilian
618 labor force greater than two million is negative for the second and third quarters (the regression
619 line shown in Figure 9 is for second quarter data). The unemployment rate combined with
620 telework policies have contributed to reduced NO_x emissions and thus lower tropNO₂ values
621 across the US. This is similar to the positive correlation between Gross Domestic Product (GDP)
622 and tropNO₂ reported by Keller et al. (2020). For reasons un-known, cities such as Phoenix, AZ,
623 Minneapolis, MN, Dallas and Houston, TX, and Chicago, IL showed no change or a slight
624 increase in tropNO₂ in 2020 compared to 2019 though unemployment rate in 2020 was much
625 higher compared to 2019. Keller et al. (2020) do not report these outliers because their analysis is
626 for all developing countries around the world and is not granular at the city level like our
627 analysis.

628 4. Discussion

629

630 The TROPOMI tropNO₂ data captures the day to day variability in tropospheric NO₂
631 concentrations but due to cloud cover and uncertainties associated with assumptions such as a
632 priori profile and lower sensitivity to near surface NO₂, on certain days the tropNO₂ retrievals do
633 not adequately represent the changes in near surface NO₂ (Ialongo et al., 2020; Cersosimo et al.,
634 2020; Goldberg et al., 2020). The tropospheric NO₂ variability is very well captured, however, on
635 monthly scales and even on weekly scales, to the extent that weekday/weekend cycles are
636 noticeable. When using the TROPOMI tropNO₂ data, we wanted to establish that it not only
637 shows the reductions/drop in tropNO₂ due to reductions in on-road NO_x emissions but that the
638 trend during the post-lockdown recovery phase can be detected as well.

639 The spatial and temporal analysis, relating indicators of human activity during and prior to
640 the COVID-19 lockdown to air quality conditions, shows that while power plant emissions
641 changes were not drastic compared to on-road emissions, the on-road emissions in the five
642 analysis cities dropped coinciding with the start date and the duration of the lockdown. The
643 changes in on-road NO_x emissions correlated with tropNO₂ changes for these five locations,
644 giving confidence in use of tropNO₂ data in other parts of the CONUS, and to draw conclusions
645 about relating changes in tropNO₂ to economic activity changes. We found that the weekday-
646 weekend differences were pronounced in on-road emissions and tropNO₂ data, and the lowest
647 values of on-road NO_x occurred on weekends even during the lockdown periods. The
648 unemployment rate and its increase during the lockdown and post lockdown period appears to
649 also be a good proxy for economic activity and is correlated well with the decrease in tropNO₂.
650 At the height of the lockdown in the second quarter of 2020, the unemployment rate increase was

651 as high as 17% in populated metropolitan areas; even at the end of the third quarter of 2020, the
652 unemployment rate increase was ~10%. The first quarter unemployment rate was constant at
653 ~5% and did not vary; it showed no relationship to tropNO₂ as expected because the impacts due
654 to the lockdown did not affect unemployment rate until the second quarter

655 The satellite data must be analyzed by considering various quality flags and understanding
656 the limitations of the algorithm. It is likely using the quality flag > 0.75 for TROPOMI tropNO₂
657 was conservative, but the extremely low daily tropNO₂ values on certain days even when on-
658 road NO_x emissions were high is indicative that the TROPOMI data are more interpretable when
659 averaged to weekly or monthly time scales. For tropNO₂ retrievals that have quality flags
660 between 0.5 and 0.75, suggesting cloud contamination, in future work, we will look at the
661 coincident high resolution (750m) VIIRS cloud mask product to analyze TROPOMI flags for
662 cloud contamination. This analysis will help improve our analysis using the daily tropNO₂
663 retrievals by either including more retrievals or removing some retrievals from the matching with
664 on-road emissions data.

665 5. Conclusions

666 It has already been established by numerous research studies that reduced traffic (on-
667 road) and industrial emissions led to improved air quality during the COVID-19 lockdown
668 measures implemented by various countries across the globe. However, most studies used
669 mobility data as a proxy for reduced human activity to interpret satellite observations of tropNO₂
670 but did not directly relate the reduced on-road emissions with reduced air quality observations.
671 Here, for the first time we directly correlate on-road NO_x emissions data to TROPOMI tropNO₂
672 in four urban and one rural area in the US. For this, we used TROPOMI tropNO₂, VIIRS AOD,

674 on-road NO_x emissions, and unemployment rates to develop a comprehensive analysis for 2019
675 and 2020. Where needed, we conducted rotated wind analyses to sample correctly and match the
676 on-road NO_x emissions with tropNO₂ data. We also developed a novel way of deseasonalizing
677 tropNO₂ data, and used changes in unemployment rate data as an indicator for economic activity.

678 Our analysis of reductions in on-road NO_x emissions from light and heavy-duty vehicles
679 derived from fuel sales data showed a reduction from 9% to 19% between February and March
680 2020. When lockdown measures were the most stringent, at the onset of the lockdown period in
681 the middle of March 2020 in most of the US and between March and April 2020, the on-road
682 NO_x emissions dropped further by 8% to 31%. These precipitous drops in NO_x emissions
683 correlated well with tropNO₂. Furthermore, the changes in tropNO₂ across the continental US
684 between 2020 and 2019 correlated well with changes in the on-road NO_x emissions (Pearson
685 correlation coefficient of 0.68) but correlated weakly with changes in emissions from power
686 plants (Pearson correlation coefficient of 0.35). These findings confirm the known fact that
687 power plants are no longer a major source of NO₂ in urban areas of the US. As the US entered
688 into a post-pandemic phase between May and November 2020, the increased mobility resulted in
689 increased NO_x emissions nearly returning to the pre-lockdown phase but not entirely back to
690 100%. Though the lockdown in most of the US ended by May, the on-road NO_x emissions did
691 not bounce back to near normal values until August; for Los Angeles and San Francisco, the on-
692 road NO_x emissions continued to be 20% below normal even in November. These changes are
693 reflected in the tropNO₂ data, with the exception that Los Angeles and San Francisco, where the
694 tropNO₂ diverged from on-road NO_x emissions trends, which needs further inquiry. The positive
695 linear correlation between on-road NO_x emissions and TROPOMI tropNO₂ ($r = 0.68$) suggests
696 that satellite tropospheric column observations of NO₂ captured the changes in on-road emissions

697 and can be used to study changes in NO_x emissions due to traffic where ground observations are
698 not available.

699 The negative correlation between changes in tropNO₂ and increased unemployment rate
700 indicates that with the increased unemployment rate combined with telework policies across the
701 US for non-essential workers, the NO₂ values decreased at the rate of 0.8 μmoles/m² per unit
702 percentage increase in the unemployment rate.

703 Across the US we found positive spatial correlation between S5P TROPOMI tropNO₂ and
704 SNPP VIIRS AOD measurements in urban regions indicating common source sectors for NO₂
705 and aerosols/aerosol precursors. We developed a new mechanism using the changes in AOD-
706 tropNO₂ slope to screen for fire events influencing aerosol concentrations in urban/industrial
707 regions that can be used to analyze changes in aerosols due to emissions reductions. The
708 COVID-19 pandemic experience has provided the scientific community an opportunity to
709 identify scenarios that can lead to a new normal urban air quality and assess if the new normal
710 can be sustained with novel policies such as increased telework and a shift towards driving
711 electric cars.

712

713

714 **Acknowledgements.** This work is part of a NOAA wide COVID-19 project funded by the
715 Joint Polar Satellite System (JPSS) and the office of Oceanic and Atmospheric Research (OAR)
716 to investigate the impact of lockdown on aerosols and trace gases including greenhouse gases.
717 The authors thank Mitch Goldberg (Chief Scientist of NOAA National Environmental Satellite
718 Data and Information Services), Greg Frost (Program Manager, NOAA Climate Program
719 Office), and Satya Kalluri (Science Advisor to the JPSS program) for securing funds for this

720 work. The authors thank the European Space Agency for the provision of the Sentinel 5
721 Precursor Tropospheric Monitoring Instrument data. The authors also thank members of NOAA
722 NESDIS JPSS aerosol calibration and validation team for the routine validation of Suomi
723 National Polar-orbiting Partnership Visible Infrared Imaging Radiometer Suite aerosol optical
724 depth product (Istvan Laszlo, Hongqing Liu, and Hai Zhang) used in our analysis. Brian
725 McDonald acknowledges the support from NOAA NRDD Project (#19533) - “COVID-19: Near
726 Real-time Emissions Adjustment for Air Quality Forecasting and Long-Term Impact
727 Analyses.” Daniel Tong acknowledges the partial support of NOAA Weather Program Office
728 (NA19OAR4590082), and Daniel Goldberg acknowledges the support of NASA RRNES grant
729 #: 80NSSC20K1122. The authors acknowledge the help of Amy Huff (IM Systems Group) in
730 proof reading the manuscript.

731 **Author Contributions.** SK conceived the scope of the scientific study and formulated the
732 analysis and wrote the manuscript. ZW conducted the scientific analyses including the
733 generation of the figures used in the manuscript. BM processed and provided the on-road NO_x
734 emissions data and wrote Section 2.2. DLG and DT conducted analysis that helped interpret the
735 features observed in TROPOMI tropospheric NO₂ data shown in Figures 4 and 5 and reviewed
736 the manuscript.

737 **Disclaimer.** The scientific results and conclusions, as well as any views or opinions expressed
738 herein, are those of the author(s) and do not necessarily reflect those of NOAA or the
739 Department of Commerce.

740 **Data Statement.** The publicly available SNPP VIIRS AOD data can be obtained from NOAA
741 CLASS (<https://www.avl.class.noaa.gov>) and the gridded Level 3 AOD data can be obtained
742 from ftp://ftp.star.nesdis.noaa.gov/pub/smcd/VIIRS_Aerosol/npp.viirs.aerosol.data/epsaot550.

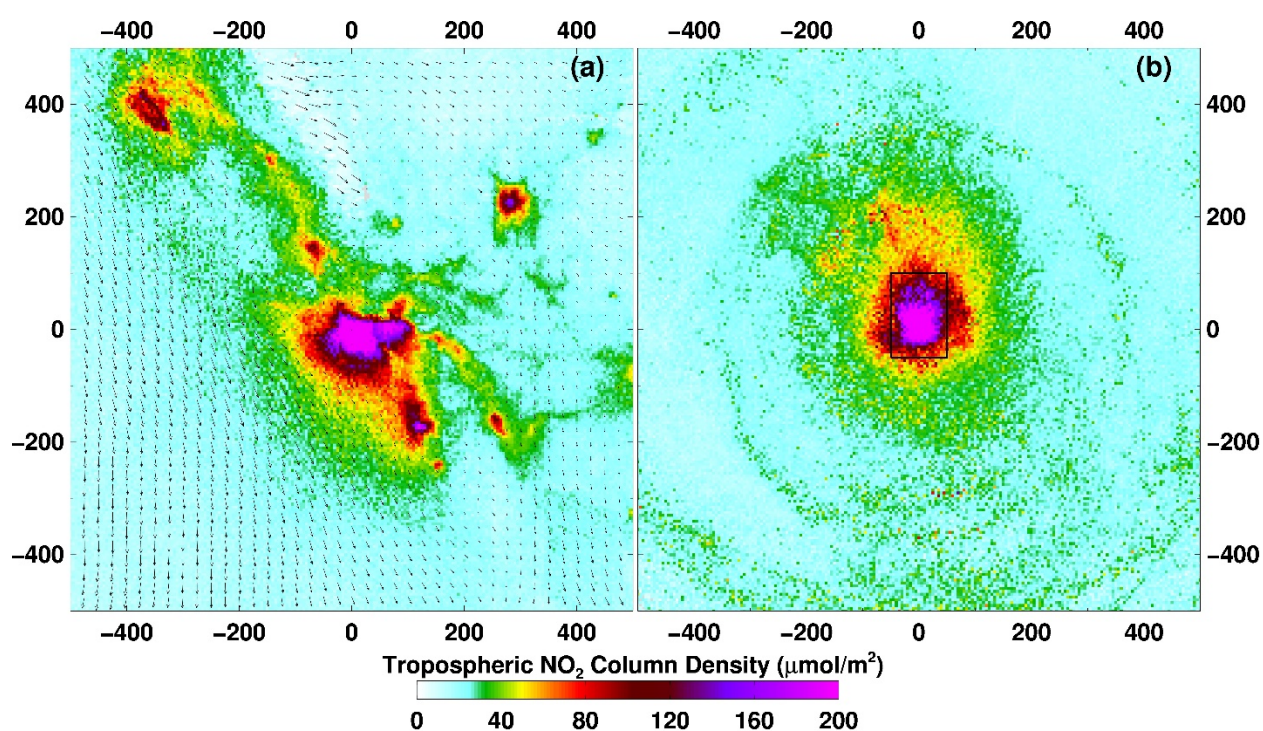
743 The Sentinel 5P TROPOMI NO₂ data can be obtained from
 744 <https://scihub.copernicus.eu/dhus/#/home>. The on-road NO_x emissions data are currently not
 745 publicly available as co-author BM's team is in the process of publishing its analyses.

746

747

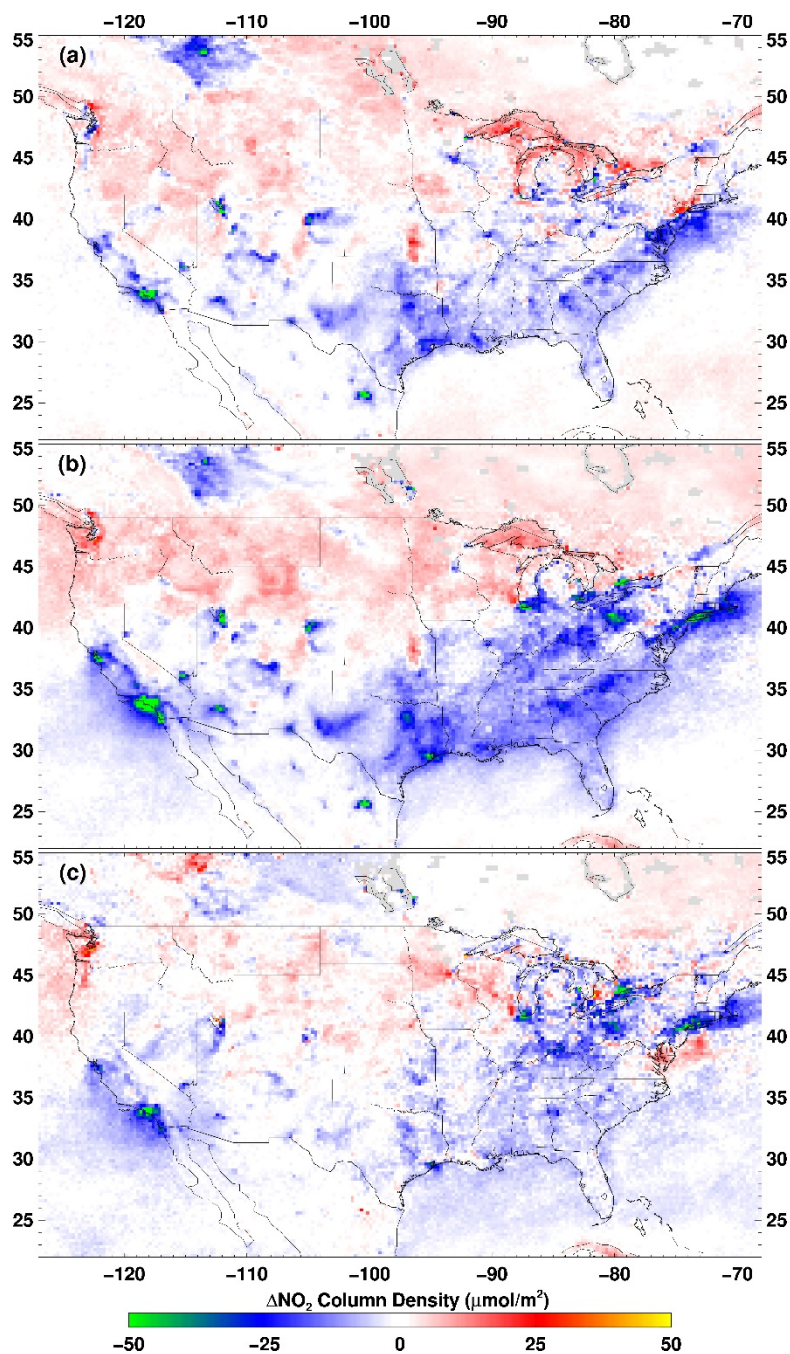
748

749



750

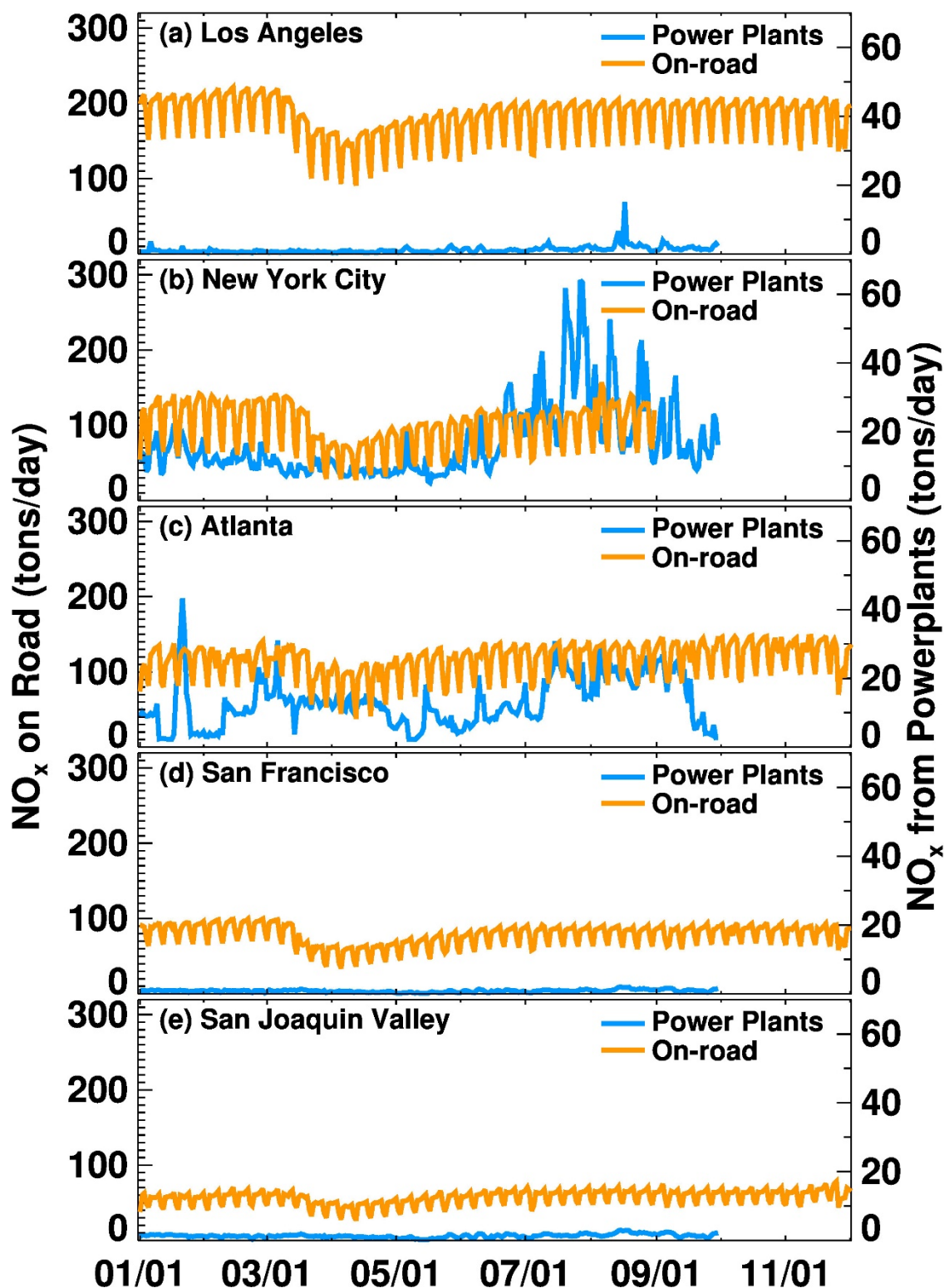
751 Figure 1: Sentinel 5P TROPOMI monthly mean tropNO₂ for January 2020 for Los Angeles. (a)
 752 Original pixel level data remapped to 5 km x 5 km resolution and averaged for the month. The
 753 monthly mean ERA5 wind vectors are overlaid on the tropNO₂ map to indicate the wind
 754 direction. (b) Remapped tropNO₂ data grids rotated in the direction of the wind using ERA5
 755 wind fields. The downwind direction is towards North (zero on the axis). For the monthly mean
 756 to be computed, we used a criterion that at least 25% of the days in a month should have
 757 retrievals. The black rectangle defines the area for which tropNO₂ data are averaged.



758

759 Figure 2: tropNO₂ changes between pre-lockdown period (January to February) and lockdown
760 period (15 March to 30 April) for (a) 2019ΔNO₂, (b) 2020ΔNO₂, and (c) the difference between
761 2020ΔNO₂ and 2019ΔNO₂. The double differencing is expected to minimize the seasonal
762 differences and provide a realistic estimate of change in tropNO₂ due to emissions changes.

763



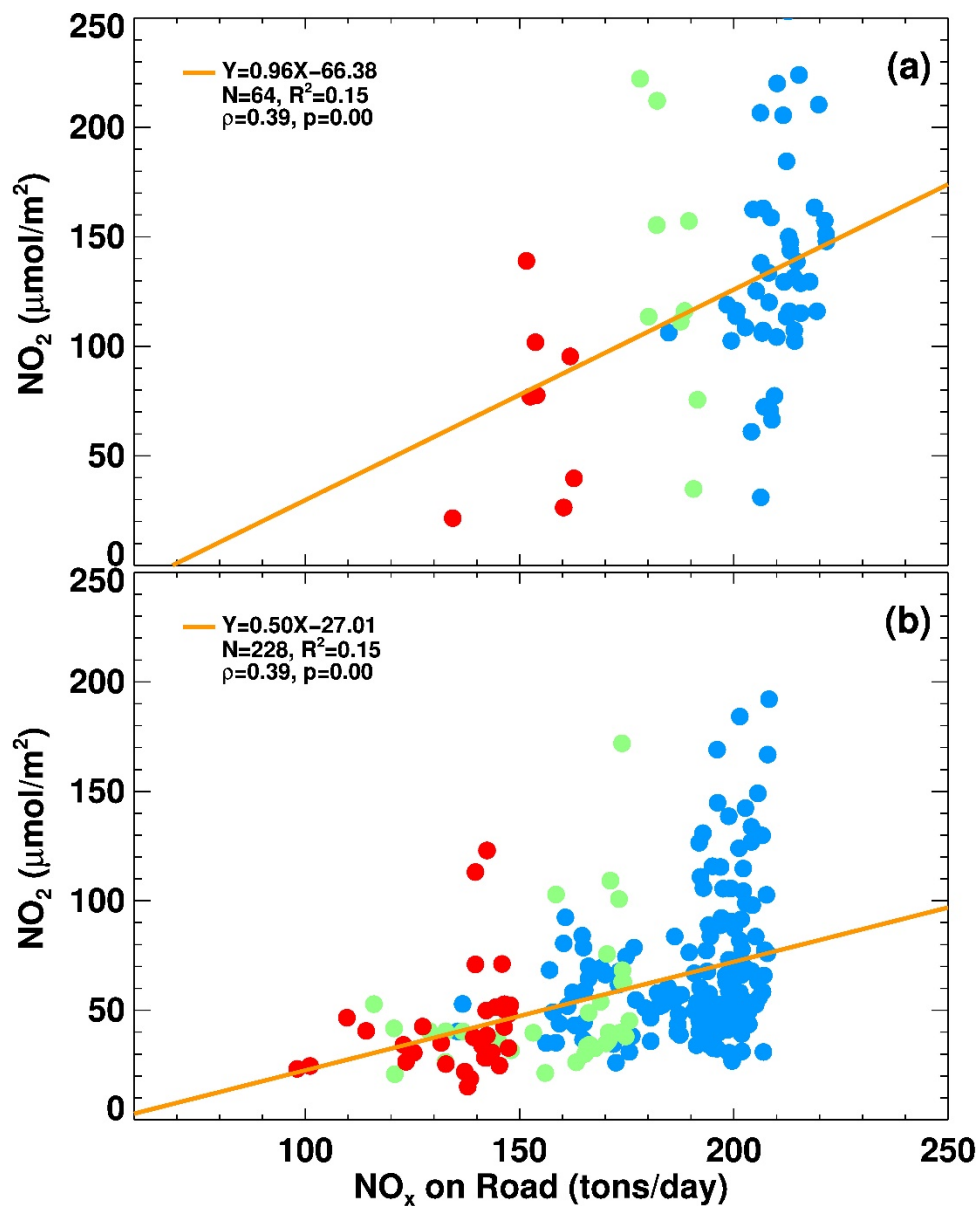
764

765 Figure 3: Time series of daily on-road and power plant NO_x emissions for different cities from
 766 January to November 2020. Note that the time series ends on 31 August for New York City
 767 because the traffic count data are not available for September to November.

768

769

770

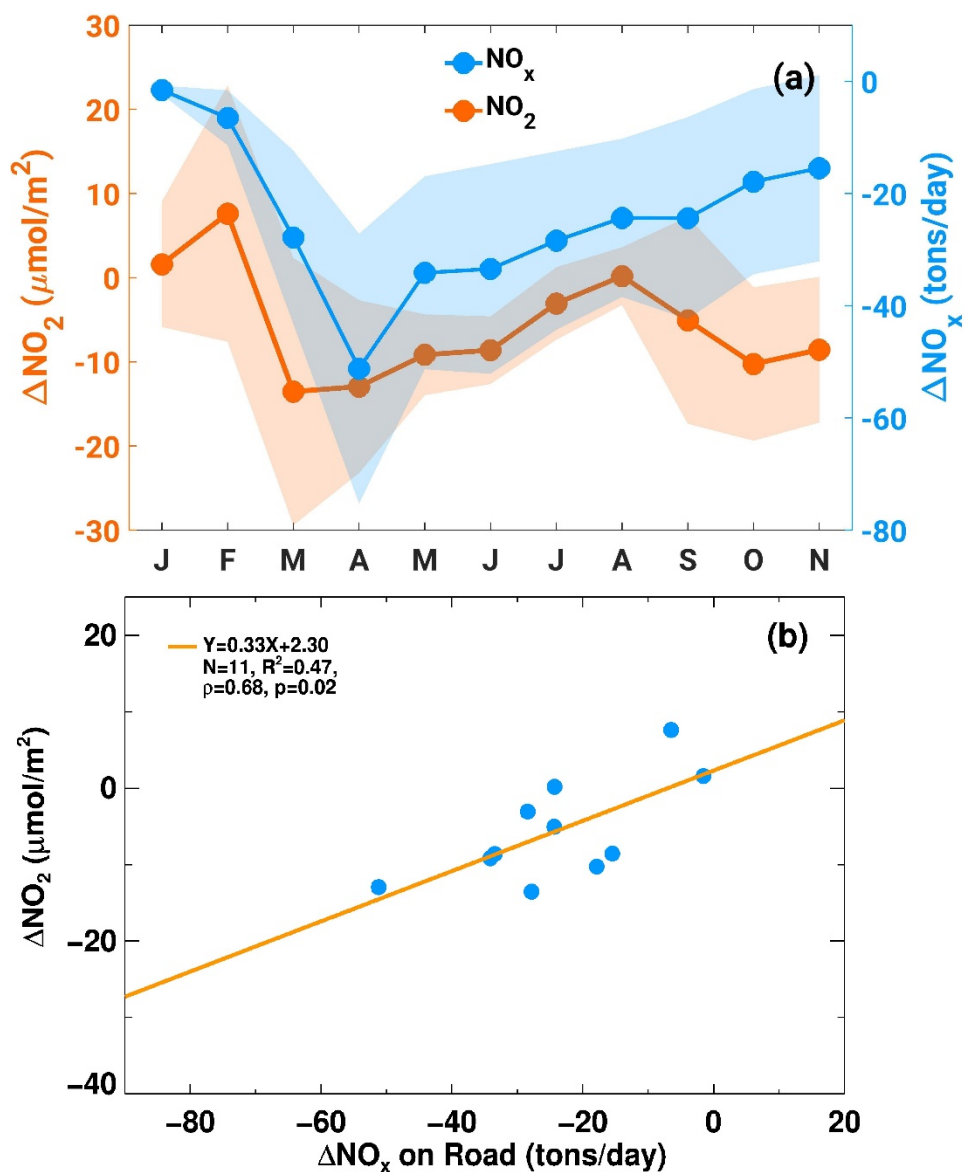
771
772

773 Figure 4: Correlation between daily trop NO_2 and daily on-road NO_x emissions for Los Angeles, CA. (a)
 774 For pre-lockdown n (January and February) and (b) For lockdown and post lockdown period (March
 775 through end of November). Red color is for data gathered on Sundays, green color is for data gathered on
 776 Saturdays, and blue color is for data gathered on weekdays.

777

778

779



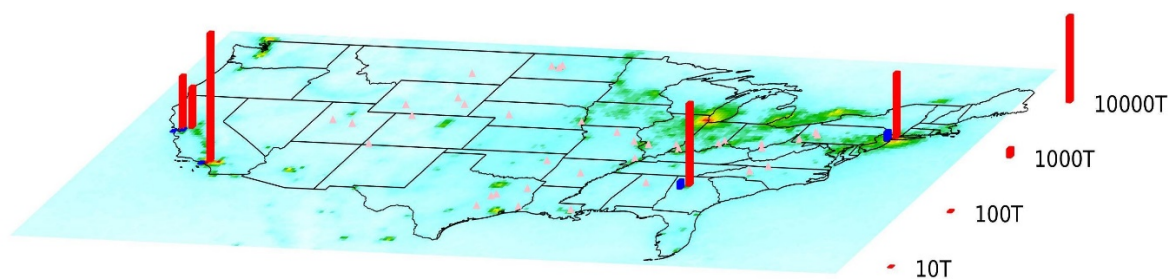
780

781

782 Figure 5: Trends in on-road monthly mean NO_x emissions (tons/day) and trop NO_2 ($\mu\text{moles}/\text{m}^2$)
 783 between 2019 and 2020 averaged for the five analysis cities. (a) Average monthly mean
 784 differences for the five cities from January to November. (b) Correlation between five-city
 785 average changes in on-road monthly mean NO_x emissions and changes in five-city average
 786 monthly mean trop NO_2

787

788



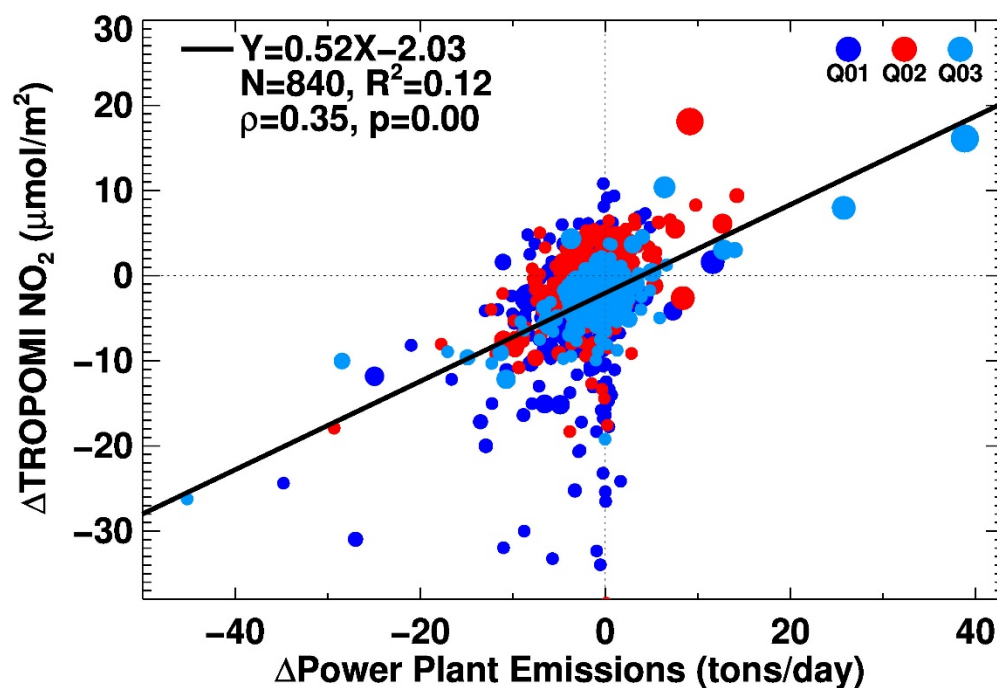
NO₂ Tropospheric Column ($\mu\text{mol}/\text{m}^2$)



789

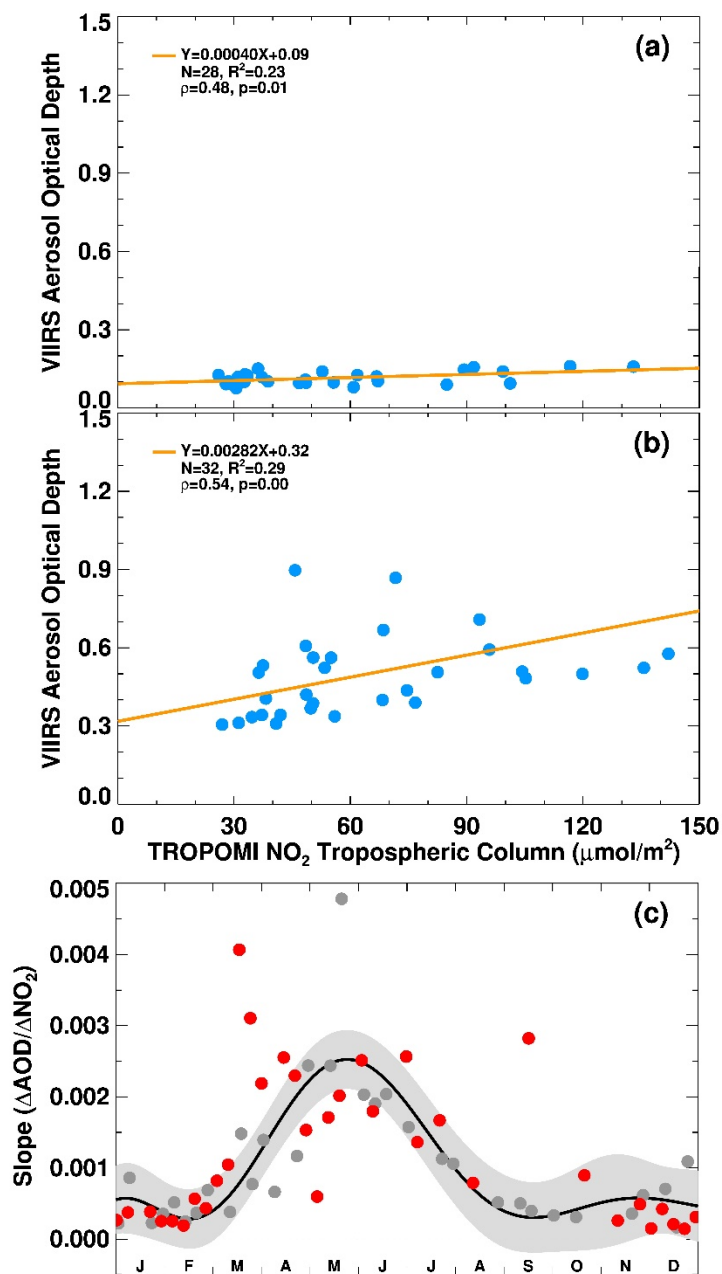
790 Figure 6: tropNO₂ map for second quarter of 2020. The red columns show total on-road NO_x
 791 emissions and the blue columns show NO_x emissions from power plants nearby these five cities
 792 (New York, Atlanta, Los Angeles, San Francisco, and San Joaquin Valley). Power plants with
 793 monthly mean NO_x emissions greater than 500 tons are also shown in the map as pink dots.

794



795

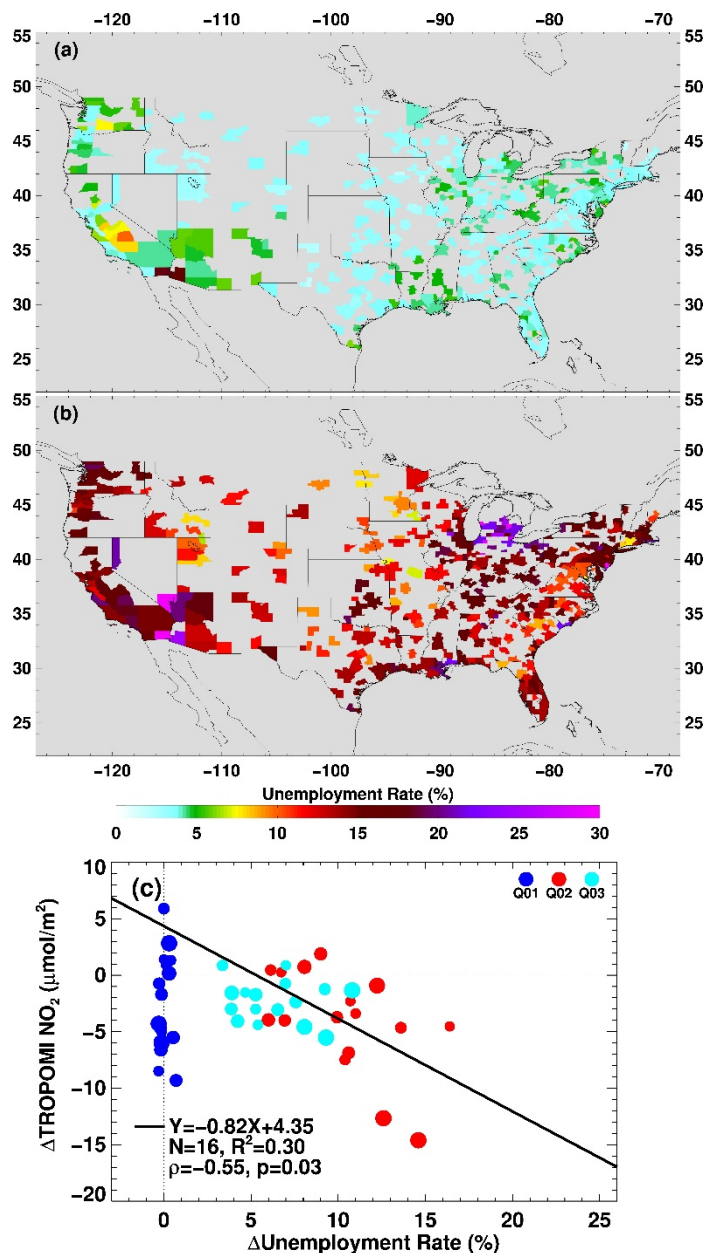
796 Figure 7: Correlation of monthly mean tropNO₂ changes between 2020 and 2019 with changes in
 797 power plant monthly mean NO_x emissions. The size of the circle indicates the magnitude of total
 798 monthly emissions (high, medium, and low) of individual power plant. To obtain monthly
 799 means, daily total NO_x emissions were added and divided by the number of days in a month to
 800 get average values in units of tons/day.



801

802

803 Figure 8: (a) Example correlation of VIIRS AOD and TROPOMI tropNO₂ during one week,
 804 September 15-21, 2019, (b) Same for September 13-19, 2020, (c) Time series of weekly slope
 805 (AOD/NO₂) with data for 2019 in gray color and data for 2020 in red color for Los Angeles,
 806 California. The black solid line is the fit to 2019 data indicating seasonal photochemistry. Any
 807 data points that depart from the shaded gray region are treated as the period when transported
 808 aerosols (e.g., smoke) influenced the air mass over Los Angeles.



809

810 Figure 9: The impact of COVID-19 lockdown on the unemployment rate in metropolitan
 811 areas and tropNO₂. (a) Unemployment rate in April 2019, (b) Unemployment rate in
 812 April 2020, and (c) Correlation between increase in unemployment between 2020 and
 813 2019 and tropNO₂ changes. Only data for metropolitan areas where the civilian labor
 814 force in 2019 was greater than two million are shown in the correlation plot. In the first
 815 quarter (Q01) unemployment changes are close to zero as pandemic impact did not begin
 816 until late March. Strong negative correlation is observed for the second (Q02) and third
 817 (Q03) quarters. The solid black line is the fit to the second quarter data.

818

819

Table 1: Ranking of cities for ozone pollution and their lockdown periods

City/Region	Ozone Pollution Ranking	Lockdown Start Date	Lockdown End Date
Los Angeles-Long Beach, CA	1	19-Mar	4-May
Visalia, CA	2	19-Mar	4-May
Bakersfield, CA	3	19-Mar	4-May
Fresno-Madera-Hanford, CA	4	19-Mar	4-May
Sacramento-Roseville, CA	5	19-Mar	4-May
San Diego-Chula Vista-Carlsbad, CA	6	19-Mar	4-May
Phoenix-Mesa, AZ	7	30-Mar	30-Apr
San Jose-San Francisco-Oakland, CA	8	19-Mar	4-May
Las Vegas-Henderson, NV	9	1-Apr	30-Apr
Denver-Aurora, CO	10	26-Mar	26-Apr
Salt Lake City-Provo-Orem, UT	11	30-Mar	13-Apr
New York-Newark, NY-NY-CT-PA*	12	22-Mar	15-May
Redding-Red Bluff, CA	13	19-Mar	4-May
Houston-The Woodlands, TX	14	2-Apr	20-Apr
El Centro, CA	15	19-Mar	4-May
Chicago-Naperville, IL-IN-WI*	16	23-Mar	1-May
El Paso-Las Cruces, TX-NM	17	2-Apr	15-May
Chico, CA	18	19-Mar	4-May
Fort Collins, CO	19	26-Mar	26-Apr
Washington-Baltimore-Arlington, DC-MD-VA-WV-PA*	20	30-Mar	15-May
Dallas-Fort Worth, TX-OK	21	2-Apr	20-Apr
Sheboygan, WI	22	24-Apr	26-May
Philadelphia-Reading-Camden, PA-NJ-DE-MD*	23	30-Mar	15-May
Milwaukee-Racine-Waukesha, WI	24	24-Apr	26-May
Hartford-East Hartford, CT	25	23-Mar	20-May

*Dates reflect the period that is the longest for any given state in the region

842

843

844

845

846

847

848

849

Table 2: Reductions in on-road NO_x emissions and tropNO₂ between 15 March to 30 April and 1 January to 29 February Derived using Double Differencing Technique						
City	2019 Δ NO _x (%)	2020 Δ NO _x (%)	Seasonality Removed On-road NO _x Emissions Changes (%) (2020 Δ NO _x - 2019 Δ NO _x)	2019 Δ NO ₂ (%)	2020 Δ NO ₂ (%)	Seasonality Removed TropNO ₂ Reductions (%) (2020 Δ tropNO ₂ - 2019 Δ tropNO ₂)
Atlanta	10.41	-17.70	-28.11	-22.67	-44.14	-21.47
San Francisco	10.54	-33.95	-44.49	-23.79	-48.18	-24.39
San Joaquin Valley	14.27	-18.39	-32.66	-27.30	-44.62	-17.32
New York City	11.04	-36.87	-47.91	-6.07	-34.05	-27.98
Los Angeles	10.57	-25.10	-35.67	-37.90	-59.68	-21.78

850

851

852

853

854

855

856

857

858

859

860

861

862

863

864

865

866

867 References

868

869 Achakulwisut, P., Brauer, M., Hystad, P., Anenberg, S. C. (2019). Global, national, and urban
870 burdens of paediatric asthma incidence attributable to ambient NO₂ pollution: estimates from
871 global datasets. *Lancet Planet Health*. 1-4, DOI: [10.1016/S2542-5196\(19\)30046-4](https://doi.org/10.1016/S2542-5196(19)30046-4)

872

873 Baidar, S., Hardesty, R. M., Kim, S.-W., Langford, A. O., Oetjen, H., Senff, C. J., et al.
874 (2015). Weakening of the weekend ozone effect over California's South Coast Air Basin:
875 Weekend ozone effect over California. *Geophysical Research Letters*, 42, 9457–9464. doi:
876 10.1002/2015GL066419

877

878 Bauwens, M., Compernelle, S., Stavrakou, T., Muller, J.-F., van Gent, J., Eskes, H., Levelt, P. F.,
879 Van der A. R., Veeffkind, P., Vlietinck, J., Yu, H., Zehner, C. (2020). Impact of Coronavirus
880 Outbreak on NO₂ Pollution Assessed Using TROPOMI and OMI Observations. *Geophysical*
881 *Research Letters*. doi: 10.1029/2020GL087978

882

883 Bishop, G. A., and Stedman, D. H. (2014), The recession of 2008 and its impact on light-duty
884 vehicle emissions in three western United States cities, *Environ Sci Technol*, 48, 14822-14827,
885 doi:10.1021/es5043518.

886

887

888 Cersosimo, A., Serio, C., Masiello, G. (2020). TROPOMI NO₂ Tropospheric Column Data:
889 Regridding to 1 km Grid-Resolution and Assessment of their Consistency with In Situ Surface
890 Observations. *Remote Sens.*, 12, 2212. <https://doi.org/10.3390/rs12142212>

891

892 Chan, K. L., M. Wiegner, J. van Geffen, I. De Smedt, C. Alberty, Z. Cheng, S. Ye, and M.
893 Wenig, MAX-DOAS measurements of tropospheric NO₂ and HCHO in Munich and the
894 comparison to OMI and TROPOMI satellite observations (2020). *Atmos. Meas. Tech.*, 13,
895 4499–4520. <https://doi.org/10.5194/amt-13-4499-2020>

896

897 de Gouw, J.A., Parrish, D.D., Frost, G.J. and Trainer, M. (2014), Reduced emissions of CO₂,
898 NO_x, and SO₂ from U.S. power plants owing to switch from coal to natural gas with combined
899 cycle technology. *Earth's Future*, 2: 75-82. <https://doi.org/10.1002/2013EF000196>

900

901 EPA (2015), MOVES2014a (Motor Vehicle Emission Simulator), Office of Transportation and
902 Air Quality, U.S. Environmental Protection Agency.

903

904 Fioletov, V. E., McLinden, C. A., Krotkov, N., Li, C. (2015). Lifetimes and emissions
905 of SO₂ from point sources estimated from OMI. *Geophys. Res. Lett.*, 42, 1969–1976, doi:
906 10.1002/2015GL063148.

907

908 Gkatzelis, G.I., J.B. Gilman, S.S. Brown, H. Eskes, A.R. Gomes, A.C. Lange, B.C. McDonald, J.
909 Peischl, A. Petzold, C. Thompson, A. Kiendler-Scharr (2021). The Global Impacts of COVID-19

- 910 Lockdowns on Urban Air Pollution: A Review. *Elementa: Science of Anthropocene*. 9 (1):
911 00176. doi: <https://doi.org/10.1525/elementa.2021.00176>
912
- 913 Goldberg, D. L., Anenberg, S. C., Griffin, D., McLinden, C. A., Lu, Z., & Streets, D.
914 G. (2020). Disentangling the impact of the COVID-19 lockdowns on urban NO₂ from natural
915 variability. *Geophysical Research Letters*, 47,
916 e2020GL089269. <https://doi.org/10.1029/2020GL089269>
917
- 918 Goldberg, D. L., Lu, Z., Streets, D. G., de Foy, B., Griffin, D., McLinden, C. A., Lamsal, L. N.,
919 Krotkov, N. A., Eskes, H. Enhanced capabilities of TROPOMI NO₂: Estimating NO_x from
920 North American 2 cities and power plants. (2019). *Environ. Sci. Technol.*, 53, 21, 12594–12601
921 <https://doi.org/10.1021/acs.est.9b04488>
922
- 923 Harkins, C., et al. (in review). "A fuel-based method for updating mobile source emissions
924 during the COVID-19 pandemic." *Environmental Research Letters*.
925
- 926 Hassler, B., B. C. McDonald, G. J. Frost, A. Borbon, D. C. Carslaw, K. Civerolo, C. Granier, P.
927 S. Monks, S. Monks, D. D. Parrish, I. B. Pollack, K. H. Rosenlof, T. B. Ryerson, E. von
928 Schneidmesser, and M. Trainer (2016), Analysis of long-term observations of NO_x and CO in
929 megacities and application to constraining emissions inventories, *Geophys Res Lett*, 43, 9920-
930 9930, doi:10.1002/2016gl069894.
931
- 932 Hersbach, H, Bell, B, Berrisford, P, et al. The ERA5 global reanalysis. *Q J R Meteorol*
933 *Soc.* 2020; 146: 1999– 2049. <https://doi.org/10.1002/qj.3803>
934
- 935 Hoesly, R. M., Smith, S. J., Feng, L., Klimont, Z., Janssens-Maenhout, G., Pitkanen, T., Seibert,
936 J. J., Vu, L., Andres, R. J., Bolt, R. M., Bond, T. C., Dawidowski, L., Kholod, N., Kurokawa, J.-
937 I., Li, M., Liu, L., Lu, Z., Moura, M. C. P., O'Rourke, P. R., and Zhang, Q. (2018). Historical
938 (1750–2014) anthropogenic emissions of reactive gases and aerosols from the Community
939 Emissions Data System (CEDS). *Geosci. Model Dev.*, 11, 369–408.
940 <https://doi.org/10.5194/gmd-11-369-2018>
- 941 Huang, M., et al. (2014), Changes in nitrogen oxides emissions in California during 2005–2010
942 indicated from top-down and bottom-up emission estimates, *J. Geophys. Res.*
943 *Atmos.*, 119, 12,928– 12,952, doi:[10.1002/2014JD022268](https://doi.org/10.1002/2014JD022268).
- 944 Huang, J., Kondragunta, S., Laszlo, I., Liu, H., Remer, L. A., Zhang, H., Superczynski, S., Ciren,
945 P., Holben, B. N., and Petrenko, M. (2016), Validation and expected error estimation of Suomi-
946 NPP VIIRS aerosol optical thickness and Ångström exponent with AERONET, *J. Geophys. Res.*
947 *Atmos.*, 121, 7139– 7160, doi:[10.1002/2016JD024834](https://doi.org/10.1002/2016JD024834).
- 948 Iolango, I., Virta, H., Eskes, H., Hovila, J., Douros, J. (2020). Comparison of
949 TROPOMI/Sentinel 5 Precursor NO₂ observations with ground-based measurements in Helsinki,
950 *Atmos. Meas. Tech.*, 13, 205–218, <https://doi.org/10.5194/amt-2019-329>

- 951 Jiang, Z., B. C. McDonald, H. Worden, J. R. Worden, K. Miyazaki, Z. Qu, D. K. Henze, D. B. A.
952 Jones, A. F. Arellano, E. V. Fischer, L. Y. Zhu, and K. F. Boersma (2018), Unexpected
953 slowdown of US pollutant emission reduction in the past decade, *P Natl Acad Sci USA*, 115,
954 5099-5104, doi:10.1073/pnas.1801191115.
- 955
- 956 Judd, L. M., Al-Saadi, J. A., Szykman, J. J., Valin, L. C., Janz, S. J., Kowalewski, M. G., Eskes,
957 H. J., Veefkind, J. P., Cede, A., Mueller, M., Gebetsberger, M., Swap, R., Pierce, R. B., Nowlan,
958 C. R., Abad, G. G., Nehrir, A., and Williams, D. (2020). Evaluating Sentinel-5P TROPOMI
959 tropospheric NO₂ column densities with airborne and Pandora spectrometers near New York
960 City and Long Island Sound, *Atmos. Meas. Tech.*, 13, 6113–6140, [https://doi.org/10.5194/amt-](https://doi.org/10.5194/amt-13-6113-2020)
961 [13-6113-2020](https://doi.org/10.5194/amt-13-6113-2020)
- 962 Keller, C. A., Evans, M. J., Knowland, K. E., Hasenkopf, C. A., Modekurty, S., Lucchesi, R. A.,
963 Oda, T., Franca, B. B., Mandarino, F. C., Díaz Suárez, M. V., Ryan, R. G., Fakes, L. H., and
964 Pawson, S. (2020). Global Impact of COVID-19 Restrictions on the Surface Concentrations of
965 Nitrogen Dioxide and Ozone, *Atmos. Chem. Phys. Discuss.* [preprint],
966 <https://doi.org/10.5194/acp-2020-685>, in review.
- 967
- 968 Kim, S.-W., McDonald, B. C., Baidar, S., Brown, S. S., Dube, B., Ferrare, R. A., Frost, G.
969 J., Harley, R. A., Holloway, J. S., Lee, H.-J., et al. (2016), Modeling the weekly cycle of
970 NO_x and CO emissions and their impacts on O₃ in the Los Angeles-South Coast Air Basin during
971 the CalNex 2010 field campaign, *J. Geophys. Res. Atmos.*, 121, 1340–1360,
972 doi:[10.1002/2015JD024292](https://doi.org/10.1002/2015JD024292).
- 973
- 974 Kondragunta, S., D. Crisp, and C. Zehner (2020), Disseminating scientific results in the age of
975 rapid communication, *Eos*, 101, <https://doi.org/10.1029/2020EO150710>. Published on 20
976 October 2020.
- 977
- 978 Kroll, J.H., Heald, C.L., Cappa, C.D. *et al.* The complex chemical effects of COVID-19
979 shutdowns on air quality. *Nat. Chem.* 12, 777–779 (2020). [https://doi.org/10.1038/s41557-020-](https://doi.org/10.1038/s41557-020-0535-z)
980 [0535-z](https://doi.org/10.1038/s41557-020-0535-z)
- 981
- 982 Lamsal, N. L., Duncan, B.N., Yoshida, Y., Krotkov, N. A., Pickering, K. E., Streets, D. (2015).
983 U.S. NO₂ trends (2005–2013): EPA Air Quality System (AQS) data versus improved
984 observations from the Ozone Monitoring Instrument (OMI), *Atmospheric Environment*, 100,
985 130-143.
- 986 Laszlo, I. and Liu, H., 2016. EPS Aerosol Optical Depth (AOD) Algorithm Theoretical Basis
987 Document, version 3.0.1, June 28, 2016, NOAA NESDIS.
- 988
- 989 Levy, R.C., Remer, L.A., Mattoo, S., Vermote, E.F., and Kaufman, Y.J. (2007). Second-
990 generation operational algorithm: retrieval of aerosol properties over land from inversion of

- 991 Moderate Resolution Imaging Spectroradiometer spectral reflectance. *J Geophys Res.*, *112*.
992 doi:10.1029/2006JD007811
- 993 Lin, J.-T., Martin, R. V., Boersma, K. F., Sneep, M., Stammes, P., Spurr, R., Wang, P., Van
994 Roozendael, M., Clémer, K., and Irie, H. (2014). Retrieving tropospheric nitrogen dioxide from
995 the Ozone Monitoring Instrument: effects of aerosols, surface reflectance anisotropy, and vertical
996 profile of nitrogen dioxide, *Atmos. Chem. Phys.*, *14*, 1441–1461. [https://doi.org/10.5194/acp-14-](https://doi.org/10.5194/acp-14-1441-2014)
997 1441-2014
- 998 Liu, F., Page, A., Strode, S. A., Yoshida, Y., Choi, S., Zheng, B., Lamsal, L., Li, C., Krotkov, N.
999 A., Eskes, H., van der, R., Veefkind, P., Levelt, P. F., Hauser, O. P., Joiner, J. (2020). Abrupt
1000 decline in tropospheric nitrogen dioxide over China after the outbreak of COVID-19, *Science*
1001 *Advances*, *6*, 28, eabc2992. DOI: 10.1126/sciadv.abc2992
- 1002 Liu, F. et al. (2021). Abrupt decline in tropospheric nitrogen dioxide after the outbreak of
1003 COVID-19. Paper presented at 101st virtual American Meteorological Association meeting.
- 1004 Liu, M., J. Lin, H. Kong, K. F. Boersma, H. Eskes, Y. Kanaya, Q. Hes, X. Tian, K. Qin, P. Xie,
1005 R. Spurr, R. Ni, Y. Yan, H. Weng, J. Wang (2020). A new TROPOMI product for tropospheric
1006 NO₂ columns over East Asia with explicit aerosol corrections. *Atmos. Meas. Tech.*, *13*, 4247–
1007 4259. <https://doi.org/10.5194/amt-13-4247-2020>
- 1008 Lorente, A., Boersma, K.F., Eskes, H.J. *et al.* Quantification of nitrogen oxides emissions from
1009 build-up of pollution over Paris with TROPOMI. *Sci Rep* **9**, 20033 (2019).
1010 <https://doi.org/10.1038/s41598-019-56428-5>
- 1011 Mazuuca, G. M., X. Ren, C. P. Loughner, M. Estes, J. H. Crawford, K. E. Pickering, A. J.
1012 Weinheimer, and R. R. Dickerson, Ozone production and its sensitivity to NO_x and VOCs:
1013 results from the DISCOVER-AQ field experiment, Houston 2013. 2016. *Atmos. Chem. Phys.*,
1014 *16*, 14463–14474. doi: 10.5194/acp-16-14463-2016
- 1015 McDonald, B. C., S. A. McKeen, Y. Y. Cui, R. Ahmadov, S. W. Kim, G. J. Frost, I. B. Pollack,
1016 T. B. Ryerson, J. S. Holloway, M. Graus, C. Warneke, J. B. Gilman, J. A. de Gouw, J. Kaiser, F.
1017 N. Keutsch, T. F. Hanisco, G. M. Wolfe, and M. Trainer (2018), Modeling ozone in the Eastern
1018 U.S. using a fuel-based mobile source emissions inventory, *Environ Sci Technol*, *52*, 7360-7370,
1019 doi:10.1021/acs.est.8b00778.
- 1020 McDonald, B. C., T. R. Dallmann, E. W. Martin, and R. A. Harley (2012), Long-term trends in
1021 nitrogen oxide emissions from motor vehicles at national, state, and air basin scales, *J Geophys*
1022 *Res-Atmos*, *117*, D00V18, doi:10.1029/2012jd018304.
- 1023
- 1024 McDonald, B. C., Z. C. McBride, E. W. Martin, and R. A. Harley (2014), High-resolution
1025 mapping of motor vehicle carbon dioxide emissions, *J Geophys Res-Atmos*, *119*, 5283-5298,
1026 doi:10.1002/2013jd021219.

- 1027 McDonald, B. C., Dallmann, T. R., Martin, E. W., and Harley, R. A. (2012), Long-term trends in
1028 nitrogen oxide emissions from motor vehicles at national, state, and air basin scales, *J. Geophys.*
1029 *Res.*, 117, D00V18, doi: 10.1029/2012JD018304
- 1030 McDonald, B. C., et al. (2018). Volatile chemical products emerging as largest petrochemical
1031 source of urban organic emissions. *Science* 359, 760-764.
- 1032 Naeger, A.R. and Murphy, K. (2020). Impact of COVID-19 Containment Measures on Air
1033 Pollution in California. *Aerosol Air Qual. Res.* <https://doi.org/10.4209/aaqr.2020.05.0227>
- 1034 Parker, H. A., Hasheminassab, S., Crouse, J. D., Roehl, C. M., & Wennberg, P. O. (2020).
1035 Impacts of traffic reductions associated with COVID-19 on Southern California air quality.
1036 *Geophysical Research Letters*, 47, e2020GL090164. <https://doi.org/10.1029/2020GL090164>
1037
- 1038 Qin, M., Murphy, B.N., Isaacs, K.K. *et al.* (2021). Criteria pollutant impacts of volatile chemical
1039 products informed by near-field modelling. *Nat Sustain* 4, 129–137.
1040 <https://doi.org/10.1038/s41893-020-00614-1>
- 1041 Schiferl, L. D., C. L. Heald, J. B. Nowak, J. S. Holloway, J. A. Neuman, R. Bahreini, I. B.
1042 Pollack, T. B. Ryerson, C. Wiedinmyer, and J. G. Murphy (2014), An investigation of ammonia
1043 and inorganic particulate matter in California during the CalNex campaign, *J. Geophys. Res.*
1044 *Atmos.*, 119, 1883–1902, doi:10.1002/2013JD020765
- 1045 Silver, B., X. He, S. Arnold, D. V. Spracklen, The impact of COVID-19 control measures on air
1046 quality in China. (2020). *Environ. Res. Lett.* 15, 084021. [https://doi.org/10.1088/1748-
1047 9326/aba3a2](https://doi.org/10.1088/1748-9326/aba3a2)
- 1048 Silvern, R. F., D. J. Jacob, L. J. Mickley, M. P. Sulprizio, K. R. Travis, E. A. Marais, R. C.
1049 Cohen, J. L. Laughner, S. Choi, J. Joiner, and L. N. Lamsal, Using satellite observations of
1050 tropospheric NO₂ columns to infer long-term trends in US NO_x emissions: the importance of
1051 accounting for the free tropospheric NO₂ background. (2019). *Atmos. Chem. Phys.*, 19, 8863–
1052 8878. <https://doi.org/10.5194/acp-19-8863-2019>
- 1053 Straka, W. III, S. Kondragunta, Z. Wei, H. Zhang, S. D. Miller, A. Watts, Examining the
1054 Economic and Environmental Impacts of COVID-19 Using Earth Observation Data. (2021).
1055 *Remote Sensing*. 13(1):5.
1056
- 1057 Tack, F., A. Merlaud, A. C. Meir, T. Vlemmix, T. Ruhtz, M-D. Iordache, X. Ge, / van der War.
1058 D/ Schuettmeyer, M. Ardelean, A. Calcan, D. Constantin, A. Schonhardt, K. Meuleman, A.
1059 Richter, and M. V. Roozendae, Intercomparison of four airborne imaging DOAS systems for
1060 tropospheric NO₂ mapping – the AROMAPEX campaign. (2019). *Atmos. Meas. Tech.*, 12, 211–
1061 236. <https://doi.org/10.5194/amt-12-211>
- 1062 Today in energy, <https://www.eia.gov/todayinenergy/detail.php?id=37752>, December 11, 2018

- 1063 Tong, D., L. Pan, W. Chen, L. Lamsal, P. Lee, Y. Tang, H. Kim, S. Kondragunta, I. Stajner,
1064 Impact of the 2008 Global Recession on air quality over the United States: Implications for
1065 surface ozone levels from changes in NO_x emissions. (2016). *Geophys. Res. Lett.*,
1066 [10.1002/2016GL069885](https://doi.org/10.1002/2016GL069885)
- 1067 Tong, D.Q., L. Lamsal, L. Pan, C. Ding, H. Kim, P. Lee, T. Chai, and K.E. Pickering, and I.
1068 Stajner, Long-term NO_x trends over large cities in the United States during the 2008 Recession:
1069 Intercomparison of satellite retrievals, ground observations, and emission inventories. (2015).
1070 *Atmospheric Environment*, 107, 70-84. doi:10.1016/j.atmosenv.2015.01.035
- 1071
1072 van Geffen, J., H. J. Eskes, K. F. Boersma, J. D. Maasakkers, and J. P. Veefkind, TROPOMI
1073 ATBD of the total and tropospheric NO₂ data products, S5P-KNMI-L2-0005-RP, v1.4.0, 2019
- 1074
- 1075 Vadrevu, K. P., A. Eaturu, S. Biswas et al., Spatial and temporal variations of air pollution over
1076 41 cities of India during the COVID-19 lockdown period. (2020). *Sci. Rep.* 10, 16574.
1077 <https://doi.org/10.1038/s41598-020-72271-5>.
- 1078
- 1079 Zhang, H., Kondragunta, S., Laszlo, I., Liu, H., Remer, L. A., Huang, J., Superczynski, S.,
1080 and Ciren, P. (2016), An enhanced VIIRS aerosol optical thickness (AOT) retrieval algorithm
1081 over land using a global surface reflectance ratio database, *J. Geophys. Res.*
1082 *Atmos.*, 121, 10,717– 10,738, doi:[10.1002/2016JD024859](https://doi.org/10.1002/2016JD024859).
- 1083 Zhang, H., & Kondragunta, S. (2021). Daily and Hourly Surface PM_{2.5} Estimation from
1084 Satellite AOD. *Earth and Space Science*, 8,
1085 e2020EA001599. <https://doi.org/10.1029/2020EA001599>
- 1086
- 1087 Zhang, Q., Y. Pan, Y. He, W. W. Walters, Q. Ni, X. Liu, G. Xu, J. Shao, C. Jiang, Substantial
1088 nitrogen oxides emission reduction from China due to COVID-19 and its impact on surface
1089 ozone and aerosol pollution. (2021). *Science of The Total Environment*, 753.
- 1090 Zhao, X., D. Griffin, V. Fioletov, C. McLinden, A. Cede, M. Tiefengraber, M. Muller, K.
1091 Bognar, K. Strong, F. Boersma, H. Eskes, J. Davies, A. Ogyu, and S. C. Lee. (2020).
1092 Assessment of the quality of TROPOMI high-spatial-resolution NO₂ data products in the Greater
1093 Toronto Area, *Atmos. Meas. Tech.*, 13, 2131–2159. <https://doi.org/10.5194/amt-13-2131-2020>
- 1094 Zheng, H., S. Kong, N. Chen, Y. Yan, D. Liu, B. Zhu, K. Xu, W. Cao, Q. Ding, B. Lan, Z.
1095 Zhang, M. Zheng, Z. Fan, Y. Cheng, S. Zheng, L. Yao, Y. Bai, T. Zhao, S. Qi. (2020).
1096 Significant changes in the chemical compositions and sources of PM_{2.5} in Wuhan since the city
1097 lockdown as COVID-19, *Science of the Total Environment*, 739.
- 1098
- 1099